

RESEARCH ARTICLE

Impacts of sectoral, regional, species, and dayspecific emissions on air pollution and public health in Washington, DC

M. O. Nawaz^{1,*}, D. K. Henze¹, C. Harkins¹, H. Cao¹, B. Nault², D. Jo³, J. Jimenez⁴, S. C. Anenberg⁵, D. L. Goldberg⁵, and Z. Qu⁶

We present a novel source attribution approach that incorporates satellite data into GEOS-Chem adjoint simulations to characterize the species-specific, regional, and sectoral contributions of daily emissions for 3 air pollutants: fine particulate matter $(PM_{2.5})$, ozone (O_3) , and nitrogen dioxide (NO_2) . This approach is implemented for Washington, DC, first for 2011, to identify urban pollution sources, and again for 2016, to examine the pollution response to changes in anthropogenic emissions. In 2011, anthropogenic emissions contributed an estimated 263 (uncertainty: 130–444) $PM_{2.5}$ - and O_3 -attributable premature deaths and 1,120 (391–1795) NO₂ attributable new pediatric asthma cases in DC. PM_{2.5} exposure was responsible for 90% of these premature deaths. On-road vehicle emissions contributed 51% of NO_2 -attributable new asthma cases and 23% of pollution-attributable premature deaths, making it the largest contributing individual sector to DC's air pollution-related health burden. Regional emissions, originating from Maryland, Virginia, and Pennsylvania, were the most responsible for pollution-related health impacts in DC, contributing 57% of premature deaths impacts and 89% of asthma cases. Emissions from distant states contributed 34% more to PM_{2.5} exposure in the wintertime than in the summertime, occurring in parallel with strong wintertime westerlies and a reduced photochemical sink. Emission reductions between 2011 and 2016 resulted in health benefits of 76 (28-149) fewer pollution-attributable premature deaths and 227 (2-617) fewer NO₂-attributable pediatric asthma cases. The largest sectors contributing to decreases in pollutionrelated premature deaths were energy generation units (26%) and on-road vehicles (20%). Decreases in NO₂-attributable pediatric asthma cases were mostly due to emission reductions from on-road vehicles (63%). Emission reductions from energy generation units were found to impact PM_{2.5} more than O₃, while on-road vehicle emission reductions impacted O₃ proportionally more than PM_{2,5}. This novel method is capable of capturing the sources of urban pollution at fine spatial and temporal scales and is applicable to many urban environments, globally.

Keywords: Ozone, Nitrogen dioxide, Particulate matter, Atmospheric modeling, Source attribution, Washington, DC

1. Introduction

International, national, and local governments share the common sustainability goal of reducing the environmental and public health burdens of poor urban air quality.

*Corresponding author: Email: muhammad.nawaz@colorado.edu The "Global Health Observatory," from the World Health Organization (2021), currently estimates that 91% of the world's population is exposed to unhealthy levels of air pollution. As countries around the world rapidly urbanize (United Nations et al., 2019), the proportion of the global population exposed to unhealthy levels of urban air pollution increases. Cities must develop effective and informed air pollution control policies to reduce the major negative effects of pollution and to meet target goals for sustainability. The United States regulates air quality through National Ambient Air Quality Standards (NAAQS) for many criteria air pollutants including fine particulate matter (PM_{2.5}), ozone (O₃), and nitrogen dioxide (NO2; U.S. Environmental Protection Agency [EPA], 2014). Locally, cities like Washington, DC, or "DC" for short, are able to enact more aggressive policy on air

¹ Department of Mechanical Engineering, University of Colorado Boulder, Boulder, CO, USA

²Aerodyne Research Inc., Billerica, MA, USA

³National Center for Atmospheric Research, Boulder, CO, USA

⁴Department of Chemistry, University of Colorado Boulder, Boulder, CO, USA

⁵Milken Institute School of Public Health, George Washington University, Washington, DC, USA

⁶ John A. Paulson School of Engineering, Harvard University, Cambridge, MA, USA

quality reductions; for example, the Sustainable DC 2.0 plan (DC Office of Planning [DC OP] and DC Department of Energy and Environment [DC DOEE], 2018) specifically targets air pollution reduction from the transportation sector and considers the direct impacts of pollution exposure in its health goals.

In this study, we will use "DC" or "the district" to refer to the federal district, the "DC–MD–VA region" to refer to the U.S. EPA NAAQS attainment region, and the "DC metropolitan region" to refer to the larger surrounding region.

The aforementioned sustainability goals of DC build upon multiple decades of improving air quality. For annual averaged PM_{2.5}, as distinct from total suspended particles and PM₁₀, primary and secondary NAAQS were first established in 1997 (U.S. EPA, 2014) at a concentration of 15.0 μ g/m³. PM_{2.5} in the DC-MD-VA region was in nonattainment of this standard until 2005, when concentrations fell below the NAAQS and have since remained below the standard despite the introduction of additional stricter near-road monitoring standards in 2012 (DC DOEE, 2019). O₃ pollution has been a greater issue in the region; since 1997, the primary and secondary NAAQS for O₃ has been the "annual fourth-highest daily maximum 8-hr concentration" with standards set at 80 ppb, 75 ppb, and 70 ppb in 1997, 2008, and 2015, respectively (U.S. EPA, 2015). The region was designated as in moderate nonattainment of the 1997 standard in 2004 and improved to marginal nonattainment when considered under the 2008 standard. Currently, under the stricter 2015 standard, the region has been designated as in marginal nonattainment; under the old 2008 standard, the region is now in attainment (DC DOEE, 2019). One of the major drivers of poor O₃ mole fractions in DC and the surrounding area is the bay breeze (He et al., 2014; Loughner et al., 2014; Stauffer et al., 2015; Sullivan et al., 2019) which recirculates pollutants back into the city. In the DC-MD-VA region, NO₂ mole fractions have never exceeded the annual mean standards, originally established in 1971, nor the 1-h daily maximum standards established in 2010 (DC DOEE, 2019).

A number of unique sources are suspected to be responsible for the pollutant concentrations in DC; when referring ambiguously to multiple pollutants, we will use the term "concentrations" although the actual measurement unit for O₃ and NO₂ is "mole fractions." For PM_{2.5}, speciated observations can provide insight into its sources. The NARSTO 2004 assessment (McMurry et al., 2004) found the largest components of annual averaged PM_{2.5} in DC were sulfate and organic carbon, both primary and secondary, followed by smaller proportions of ammonium and nitrate. Since then, a number of coal powered electric generating units (EGUs) near DC have closed (Russell et al., 2017; Jolley et al., 2019), reducing a major source of SO₂ emissions in the region which would affect the composition. A number of studies have found that urban PM_{2.5} in the Atlantic U.S. forms predominantly secondarily. For example, one study (Jimenez et al., 2009) examined the composition of PM_{2.5} in New York City in both the winter and summer and found that roughly half of the PM_{2.5}, in both seasons, were of total oxygenated organic aerosol

(OOA), which includes both secondary and primary organic aerosol (OA), with the other half being secondary inorganic aerosol (SIA). Hydrocarbon OA, a surrogate for primary urban OA, made up about half of the total OOA in the winter and less than a quarter in the summer. Another study (Nault et al., 2020) also examined New York City, for 2015, and found that in the wintertime around 17% of PM_{2.5} was anthropogenic secondary OA, 16% was primary OA, and 67% was SIA.

For O₃, precursor emissions from within the DC-MD-VA region largely come from Maryland and Virginia; only 5% of volatile organic compounds (VOCs) and 8% of nitrogen oxides (NO_x) emissions in the DC-MD-VA region are estimated to come from DC (DC DOEE, 2019). High mobile emissions of NO_x are thought to be one of the largest contributors to O₃ in DC (Goldberg et al., 2016; DC DOEE, 2019). One study (Goldberg et al., 2016) used a tagging approach across a modeling domain of the eastern United States to perform a source apportionment of O₃ for the 10 worst air quality days in July 2011 in DC. They concluded that mobile and EGU emissions, primarily from Maryland, Pennsylvania, Ohio, and Virginia, contributed the most to these high ozone days in DC. Another study (Moghani et al., 2018) considered regional emission control strategies in the Mid-Atlantic for Delaware and found that a 20% local emission reduction had no effect on O₃; however, a smaller 10% reduction across upwind states resulted in O₃ benefits between 1.9 and 2.5 ppb on average. Additionally, throughout the United States, regardless of the city or year, on-road mobile sources were estimated to make the largest anthropogenic emission contribution to O₃ (Nopmongcol et al., 2017). It was estimated that emission reductions from 2002 to 2011 resulted in 5-10 fewer ozone exceedance days in the DC metropolitan area (Loughner et al., 2020).

Exposures to the 3 air pollutants being considered here (PM_{2.5}, O₃, and NO₂) all have well-established relationships with increased risk of negative health outcomes, and regardless of their attainment statuses, concentrations of these 3 pollutants in DC exceed the minimum levels at which health impacts are observed (Burnett et al., 2014; Turner et al., 2016; Malley et al., 2017; Anenberg et al., 2018; Achakulwisut et al., 2019). PM_{2.5} exposure is associated with an increased risk of premature death from health outcomes including chronic obstructive pulmonary disorder (COPD), ischemic heart disease (IHD), lower respiratory illnesses (LRI), lung cancer (LC), type-II diabetes (T2D), and stroke (Murray et al., 2020). O₃ exposure is associated with increased risk of premature death from COPD (Anenberg et al., 2010). It should be noted the exposure metrics of "sixmonth peak averaged, 1-hr daily maximum" (Jerrett et al., 2009) and "annual averaged daily 8-hour maximum" (Turner et al., 2016) that are often used in health impact analyses of O₃ exposure differ from the metrics used within the O₃ NAAQS. NO₂ exposure—and not PM_{2.5} and O₃—is significantly associated with increased pediatric asthma incidence (Achakulwisut et al., 2019).

A number of studies have examined the health impacts of pollution exposure for DC. In 2016, an estimated 1,170 premature deaths occurred due to PM_{2.5} exposure in DC

and its surrounding metropolitan area (Anenberg et al., 2019a); this area has a population nearly 5 times larger than the population just living in the district. The results of our study consider the district exclusively and not the surrounding metropolitan area. Another study (Zhang et al., 2018) estimated that in 2010, 157 PM_{2.5}-related premature deaths and 21 O₃-related premature deaths occurred in DC. NO₂ has been estimated to be responsible for 390 new pediatric asthma cases per 100,000 children per year in DC (Achakulwisut et al., 2019). Many studies have more generally quantified health impacts by pollutants, predominantly from PM_{2.5} and O₃, throughout the United States (Goodkind et al., 2019; Davidson et al., 2020; Dedoussi et al., 2020).

Urban-scale health impact analyses require pollutant exposures that can be estimated through a variety of methods. Air quality models can simulate pollutant concentrations over large areas; however, they often fail to accurately capture urban-scale spatial variability due to the coarseness of their resolution (Punger and West, 2013; Ridder et al., 2014) and often have biases as they are tailored to be accurate across large spatial extents. Remote-sensing-derived concentrations can provide global or regional pollutant coverage at resolutions that are much finer than models across similar sized domains, and remote sensing data can be incorporated into air quality models through satellite downscaling (Lacey et al., 2017; Cooper et al., 2020; Nawaz and Henze, 2020) to improve the resolution and accuracy of exposure estimates. Here, we introduce a novel method of incorporating satellite downscaling into model-estimated exposure metrics for PM_{2.5} and NO₂. In doing so, source attributions of pollutant exposures benefit from the improved accuracy of satellite-based corrections.

Source apportionment methods can use both in situ measurements and air quality models to identify the sources of pollutant exposures. Classification approaches, like positive matrix factorization (Thurston et al., 2011), involve the measurement of multiple source types prior to the measurement of the components of a receptor, like PM_{2.5}. Chemical transport model tagging approaches (Goldberg et al., 2016) track emissions from aggregated classes of sources. These 2 approaches are capable of identifying a limited number of predefined regional and sectoral sources across a single time period. If a source apportionment at a finer temporal or spatial resolution is needed; however, it can become labor intensive, experimentally challenging, or computationally expensive to identify contributions in these ways. Adjoint model sensitivity analysis is an alternative approach (Pappin and Hakami, 2013; Lee et al., 2015) for efficiently calculating the response of a small number of pollutant exposure metrics to a very large numbers of sources, which can be useful for the tailoring of cities' air quality and health goals.

In this study, we present a high-resolution, satellite-constrained source attribution for DC. We leverage remote-sensing-derived surface-level data for PM_{2.5} and NO₂ along with simulated surface mole fractions of O₃ to assess urban-scale pollution-related health impacts. We incorporate remote-sensing-derived concentrations into

adjoint sensitivity analyses (Henze et al., 2007; Zhang et al., 2015) to calculate the unique contributions from individual emission species and sectors across the continental United States on a daily basis at a $0.1^{\circ} \times 0.1^{\circ}$ spatial resolution for 3 different air pollutants: PM_{2.5}, O₃, and NO₂. We present source apportionments for 2 health impacts: air pollution-related premature deaths and new pediatric asthma cases to compare pollutants and characterize the sources of health impacts and benefits more directly. We compare results for 2011 and 2016 to quantify how pollutant exposures, health impacts, and source contributions have changed in DC across this 5-year period. The uniqueness of this approach derives from its ability to characterize the impact of anthropogenic emissions from a single day on multiple pollutant exposures and their associated health impacts. Although this method fails to capture intracity contributions as well as regional models, the value of the approach demonstrated here is that it can be applied without the need for high-resolution, computationally expensive, regional modeling, which affords application to other cities throughout the globe where regional models are unavailable or less accurate.

2. Methodology

2.1. Pollutant surface concentrations

To improve the agreement between model-simulated pollutant concentrations and in situ observations, we incorporate remote-sensing-derived surface levels of PM_{2.5} concentrations and NO₂ mole fractions into the adjoint simulations. For estimating annual PM_{2.5}, we use the values from the satellite-derived product of van Donkelaar et al. (2016) for 2011. In recent years, multiple new satellitederived PM_{2.5} estimates (Shaddick et al., 2018; Hammer et al., 2020) have emerged that extend beyond the data set used here in terms of methodology or resolution. While significant differences arise in other parts of the world, the updates over North America are more modest, in the range of 2–5 ug/m³. Regardless, we find good agreement between the van Donkelaar et al. (2016) values and the in situ AQS measurements (normalized mean bias [NMB] of 22.2%) in the DC area. For NO_2 , we oversample columns from the TROPOspheric Monitoring Instrument (TROPO-MI) between May 2018 and June 2019 to get an annual averaged equivalent product with complete coverage across our domain. The TROPOMI data used here currently represent the state-of-the science for NO₂ remote sensing. We chose this period because TROPOMI columns were unavailable during our study year, and while columns from the Ozone Monitoring Instrument (OMI) were available, the spatial resolution of the latter is much coarser (13 km \times 25 km) than that of TROPOMI. The oversampling of the TROPOMI NO₂ columns is done at $0.01^{\circ} \times 0.01^{\circ}$ resolution. These TROPOMI columns are then further converted to surface mole fractions following a methodology (Cooper et al., 2020) that is outlined in Section 2.3. We convert columns to surface mole fractions because NO₂ exposures are calculated using surface mole fractions. Hourly O_3 mole fractions were simulated for a year using a forward model simulation of GEOS-Chem; the 1-h max values for each day in the 6-month peak O₃ period were

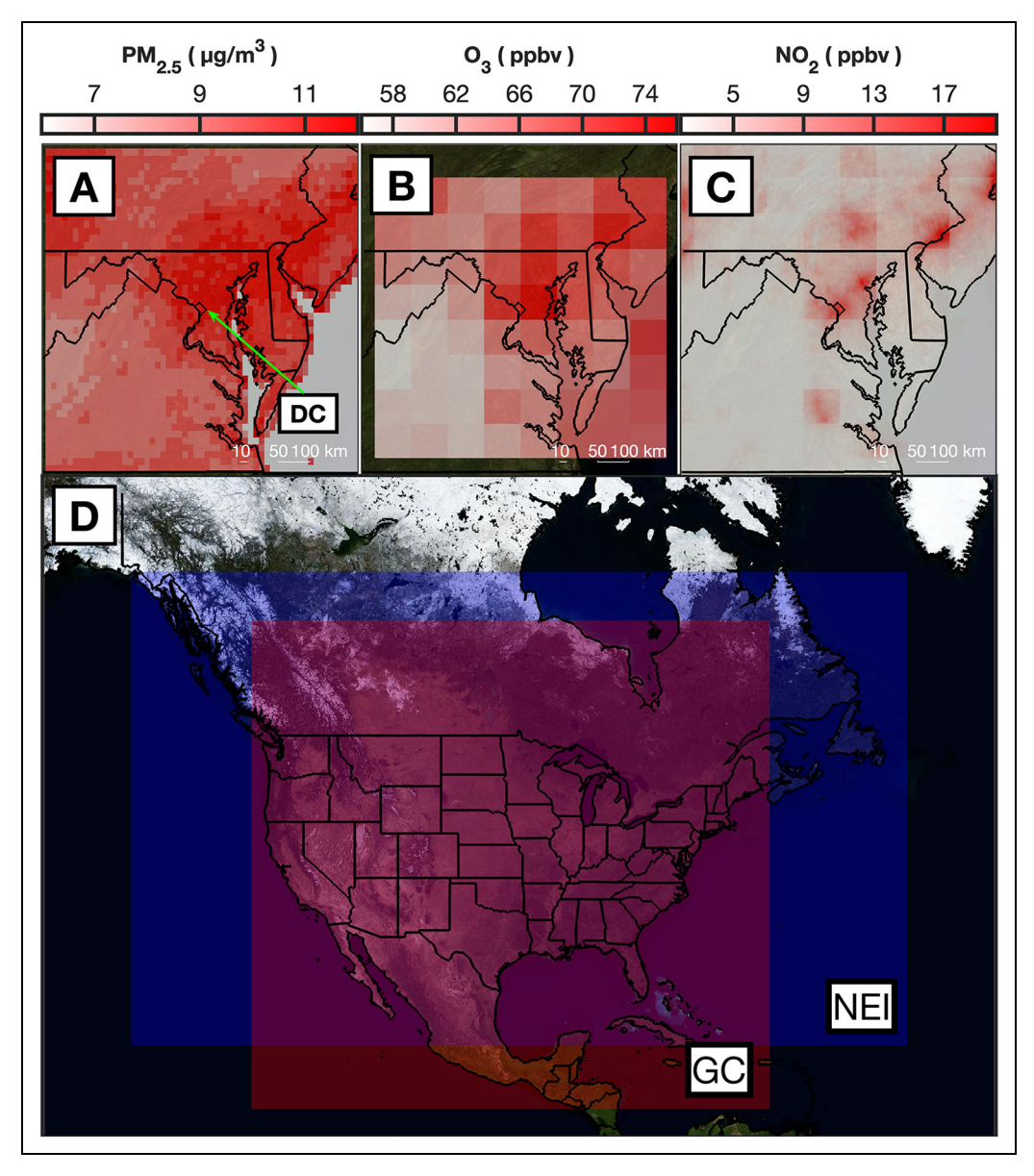


Figure 1. Surface-level concentrations of pollutants and model and emission domains. Surface-level concentrations of PM_{2.5} (A) and mole fractions of O₃ (B) and NO₂ (C) used to calculate cost functions. The concentrations for PM_{2.5} and mole fractions for NO₂ are satellite-derived while the O₃ mole fractions are model simulated. Extent of the U.S. Environmental Protection Agency National Emission Inventory (NEI) as implemented in GEOS-Chem and GEOS-Chem nested U.S. (GC) domain in blue and red, respectively (D). As referred to in the text, "purple" indicates the areas of overlap between the GEOS-Chem domain and the NEI domain. DOI: https://doi.org/10.1525/elementa.2021.00043.f1

averaged to calculate the O_3 exposure. Surface concentrations of all 3 pollutants, overlaid on top of the DC metro area, are presented in **Figure 1**. We compare simulated pollutant concentrations, along with their satellite corrected forms, against in situ observations from monitoring stations for $PM_{2.5}$, O_3 , and NO_2 in 2011. In situ data were obtained from 3 monitoring stations: the River Terrace, McMillan, and Hains Point sites for 2011.

2.2. Emissions

We use the U.S. EPA's National Emission Inventory (NEI) version 2.1 for a base year of 2011 to input anthropogenic emissions every hour in our simulation. The NEI includes emissions from northern Mexico and southern Canada.

The spatial extent of the inventory is presented in **Figure 1**. We use NEI 2011v2.1 emissions processed using the Sparse Matrix Operator Kernel Emissions (SMOKE) for GEOS-Chem (Travis et al., 2016) and input total surface emissions at the first model level and stack emissions at higher levels. We consider 16 species shown in **Table 1**. NO_x emissions are calculated by combining emissions of NO_x expressed in units of kg NO_2 , with emissions of NO_2 . GEOS-Chem considers all emissions of NO_x as NO_x ; the chemical time step of the simulation is 1 h, and so the rapid cycling between NO_x and NO_y means that there is little difference whether NO_x is emitted as NO_x or NO_y . Additionally, we calculate anthropogenic secondary organic aerosol (SOA) precursors using emissions of

Table 1. National Emissions Inventory (NEI) 2011 definitions. DOI: https://doi.org/10.1525/elementa.2021.00043.t1

Species Nitrogen oxides (NO_x), carbon monoxide (CO), sulfur dioxide (SO₂), sulfate (SO₄), ammonia (NH₃), >=C4-alkanes (ALK4), acetone (C_3H_6O), methyl ethyl ketone (C_4H_8O), propene (C_3H_6), propane (C_3H_8), formaldehyde (CH₂O), ethane (C_2H_6), acetaldehyde (C_2H_4O), primary elemental (black) carbon (BC), and primary organic carbon (OC)

Sectors Agriculture (AG), shipping (SHP), energy generation units (EGU), peaking energy generation units (EGUPK), oil and gas (OG), on-road (ONR), on-road California and Texas (ONRCATX), other point (OTHPT), industry (IND), surface (SF), and residential (RES)

Species and sector definitions for the U.S. Environmental Protection Agency NEI for base year 2011 version 2.1.

carbon monoxide (CO), benzene, toluene, and xylene following a recent update (Nault et al., 2020). For regions in our modeling domain outside of the NEI 2011 emission domain, we use the Task Force on Hemispheric Transport of Air Pollution (HTAP) emissions inventory for all anthropogenic species. This corresponds to the red, but not purple, region in **Figure 1**. For nonanthropogenic emissions, we include biogenic (Guenther et al., 2006), biomass burning (van der Werf et al., 2010), dust (Zender et al., 2003), lightning NO_x (Murray et al., 2012), soil NO_x , and other natural emissions in our simulation.

The SMOKE-processed NEIv2.1 emissions we use are separated into 11 sectors shown in **Table 1**. We denote the NEI "non-ipm point" (ptnonipm) sector as "industry" as this sector is made up of refineries, industrial plants, and waste combustors; however, aircraft emissions are also considered in this group. The "othpt" sector is made up of point sources in Canada. Nonroad emissions include emissions from recreational, construction, industrial, lawn and garden, agriculture, commercial, logging, airport support, underground mining, oilfield, recreational marine, and nonlocomotive railroad vehicles. We further subdivided the original aggregate "surface" category to isolate an "othersurface" sector. To avoid confusion within the text, we will still refer to this sector as the "surface" (SF) sector. This SF sector includes emissions from commercial cooking, non-EGU fuel combustion, gas stations, nonpoint industrial processing, solvents, waste disposal, fugitive dust, and oil and gas. We present the proportional breakdowns of subsectors for all available species in the supplemental (S1) for the SF sector. It also includes the nonplume components of EGUs, oil and gas, and industry. The "shipping" sector specifically refers to emissions from category 3 marine vessels.

Residential (RES) emissions were isolated from the surface category as follows: Using emissions from NEI 2016 version "fh," we combine the NEI 2016 sectors that make up the SF sector and determine the fraction of this sector that is made up of residential wood combustion emissions. In doing so, we get a residential fraction for each month, species, and grid cell at the $0.1^{\circ} \times 0.1^{\circ}$ spatial resolution. We then apply these residential fractions to the 2011 NEI emissions to separate the RES emissions from the surface category.

As described in Section 3.5, monthly NEI 2016 emissions are combined with our simulated source sensitivities, calculated for 2011, to quantify changes in pollutant exposures between 2011 and 2016; however, the 2016 NEI emissions have greater sectoral granularity than the 2011 NEI emissions. In order to compare these

directly, we aggregate all of the NEI 2016 subsectors into their corresponding sectors in NEI 2011 with the exception of the residential wood combustion sector, which is already disaggregated in the 2016 NEI.

In the NEI 2011, as implemented in GEOS-Chem, a number of sectors only include the in-line plume rise emissions. These sectors include EGUs, peaking EGUs, oil and gas, other point, and industry. When considering sectoral source apportionment for 2011, when referring to these sectors, we are specifically referring to the plume rise emissions. There are components of some of these sectors that are emitted at the surface level and included in the surface sector that are not considered in our definitions of the sectors. Comparing the plume rise total emissions to the totals as reported in the NEI 2011 TSD (EPA, 2015), this surface-level component for EGUs is small; however, this is not the case for the other sectors. This should be considered when interpreting results for 2011.

All 2011 sectors that contain only in-line plume rise emissions are not directly comparable to their 2016 analogues because the 2016 sectors include nonplume rise emissions that were grouped in the "surface" category in 2011. We have avoided making direct comparisons between the years for most of these sectors. For EGUs, we compare 2011 and 2016 contributions with one caveat; we consider differences in 2011 and 2016 values as lower bounds of the changes between these 2 years. While a majority of EGU emissions in 2011 were plume rise, as calculated by comparing the NEI 2011 TSD (EPA, 2015) totals to the SMOKE-processed emissions, there was a substantial component (12%) of these that were nonplume rise emissions. Given this, our estimate of 2011 EGU emissions is an underestimate; when calculating changes in emissions between 2016 and 2011, reductions calculated in this work can be thought of as a lower bound of the actual reductions that occurred for the EGU sector.

2.3. GEOS-Chem adjoint

For our source apportionment, we use the GEOS-Chem adjoint model (Henze et al., 2007) v35n for sensitivity analyses at the $0.5^{\circ} \times 0.667^{\circ}$ horizontal resolution in the nested U.S. domain. The adjoint originally corresponded to v8-02-01 of the GEOS-Chem forward model and has been updated to version 10 of the forward model. We have included additional updates (Nault et al., 2020) to incorporate a new SOA scheme in both the forward and adjoint simulations. We conduct 12 two-month adjoint simulations in 2011, for each of the 3 pollutants, and only force the adjoint for the second month, in each simulation, to

capture the impact of emissions from the first month on the second month. This requires 36 unique runs which, while computationally intensive, is feasible in contrast to the approximately 400 million runs that would be needed to conduct the same calculations using finite difference or other forward-modeling-based methods. For the December 2010 portion of the simulation, we use the NEI emissions for December 2011. We input NASA Global Modeling and Assimilation Office GEOS-5 meteorological fields for 2011.

More specifically, in this sensitivity analysis, the adjoint model calculates the gradient (λ_E) of a cost function (J) with respect to emissions (E) of distinct species at distinct grid cells and on specific days. We define unique cost functions for each of the 3 pollutants; these cost functions represent commonly used metrics for the analysis of health impacts: annual averaged population-weighted PM_{2.5} (Burnett et al., 2014), 6-month peak averaged 1-h max O₃ (Jerrett et al., 2009), and annual averaged population-weighted NO₂ (Achakulwisut et al., 2019). These 3 pollutant metrics will be referred to as "exposures" in the rest of this text. All 3 of these exposures are calculated for DC for 2011. We incorporate annual average equivalent satellite data into the PM_{2.5} and NO₂ adjoint simulations to increase the resolution of our urban-scale exposure estimates for these 2 pollutants. When exposures are calculated at too coarse of a resolution, low concentrations from less populated areas surrounding the city may be averaged into the exposure, lowering the value and underestimating health impacts (Punger and West, 2013; Ridder et al., 2014). The resolution of the exposure estimate is most critical for shorter lived species like primary PM_{2.5} and NO₂ as they are less mixed and have greater spatial variability. The lifetime of NO₂ is on the order of a day and the lifetime of PM_{2.5} is on the order of 1–2 weeks (Doherty et al., 2017), respectively. For most of the year, the lifetime of O₃ is longer; at 40° N and at the surface, O₃ lifetimes span from around 8 days in the summertime to 100 days in the wintertime (Seinfeld and Pandis, 2016).

First, we will discuss the cost function for PM_{2.5}:

$$J_{\text{PM}_{2.5}} = \frac{\sum_{i \in D} \left(P_i \times \bar{X}_I \frac{\text{sat}_i}{\text{SAT}_I} \frac{\text{SAT}_I}{\bar{X}_I^0} \right)}{\sum_{i \in D} P_i^i}.$$
 (1)

Here, i refers to spatial indexing at the $0.1^{\circ} \times 0.1^{\circ}$ resolution of the satellite-derived product and I refers to spatial indexing at the $0.5^{\circ} \times 0.667^{\circ}$ resolution of the model, \bar{X}_I represents annual averaged PM_{2.5} output from the forward model, sat_i is a satellite-derived product (van Donkelaar et al., 2016), SAT $_I$ is this same product averaged at the coarse model resolution, $P_i^{\ i}$ is a fine resolution population estimate (Center for International Earth Science Information Network, 2018), and D is the set of all grid cells within our cost function domain—in this case DC. For the purpose of calculating the adjoint forcing, we treat the ratios $\frac{\mathrm{sat}_I}{\mathrm{SAT}_I}$ and $\frac{\mathrm{SAT}_I}{\bar{X}_I^0}$ as constant; \bar{X}_I^0 is the same annual averaged PM_{2.5} output from the forward model as \bar{X}_I but is assumed to be constant when calculating the

derivative. The rescaling process is illustrated in the supplemental (S2).

Next, we consider the cost function of O₃:

$$J_{\mathcal{O}_3} = \frac{\sum_{i \in D} (P_i \times \bar{X}_I)}{\sum_{i \in D} P_i}.$$
 (2)

This cost function is similar to that of PM_{2.5} except without the satellite rescaling as there is no equivalent satellite-derived O₃ product. Here, \bar{X}_I refers to 6-month peak averaged 1-h max O₃ from the forward model.

Finally, we consider the cost function of NO₂:

$$J_{\text{NO}_2} = \frac{\sum_{i \in D} \left(P_i \times \Omega_I \times k_i \times \left(\frac{S_{\text{NO}_2}}{\Omega_I^0} \right) \times \frac{\left(\nu_i \Omega_I^0 - \Omega_I^{\text{free troposphere}} \right)}{\left(\Omega_I^0 - \Omega_I^{\text{free troposphere}} \right)} \right)}{\sum_{i \in D} P_i}.$$
(3)

Here, i refers to spatial indexing at the $0.01^{\circ} \times 0.01^{\circ}$ resolution of the satellite-derived product and I refers to spatial indexing at the $0.5^{\circ} \times 0.667^{\circ}$ resolution of the model. In applying this approach, we are assuming that the relative spatial variability of annual mean NO2 columns over the DC area has not changed significantly between 2011, the model simulation year, and 2018-2019, the TROPOMI NO₂ column years. We apply a satellite column downscaling (Cooper et al., 2020). This method makes use of 3 factors applied to simulated NO₂ columns. First, we account for subgrid variability in the lower portion of the NO₂ column to improve the horizontal resolution of our simulated columns. Second, we apply a surface to column ratio which represents the fraction of the column at the surface level and converts the column from units of $\frac{\text{molecules}}{\text{cm}^2}$ to a mixing ratio in ppbv. Lastly, we apply an urban to rural scaling factor for grid cells with column magnitudes greater than $11 \times 10^{15} \frac{\text{molecules}}{\text{cm}^2}$. This scaling factor is calculated by applying this analysis at both the surface and boundary layer and taking the ratio of the two; the factor differentiates urban and rural regimes. Here, Ω_I is the annual averaged tropospheric NO₂ column from the forward model output; we use the term Ω_I^0 to refer to the same annual averaged tropospheric NO_2 column as Ω_I but is assumed to be constant when calculating the derivative. The polluted to remote scaling term, k_i is calculated following the previously mentioned study (Cooper et al., 2020), S_{NO} , is the annual averaged forward model simulated surface NO_2 mole fractions, v_i is a spatial variability term calculated by comparing fine-resolution (0.01° × 0.01°) oversampled TROPOMI NO₂ columns to the average TROPOMI NO₂ column within the coarse-resolution (0.5° imes 0.667°) model grid box and $\Omega_I^{ ext{free troposphere}}$ is the portion of the modeled NO₂ column in the free troposphere. We assume that the overpass bias remains constant throughout the whole day and thus use it to characterize fine spatial variability, v_i , in the daily model simulated columns. The NO2 downscaling procedure is illustrated in **Figure 2**; κ (panel 1) is κ_i , surface to column (panel 2) is $\left(\frac{S_{NO_2}}{\Omega_I}\right)$, lower column variability (panel 3) is

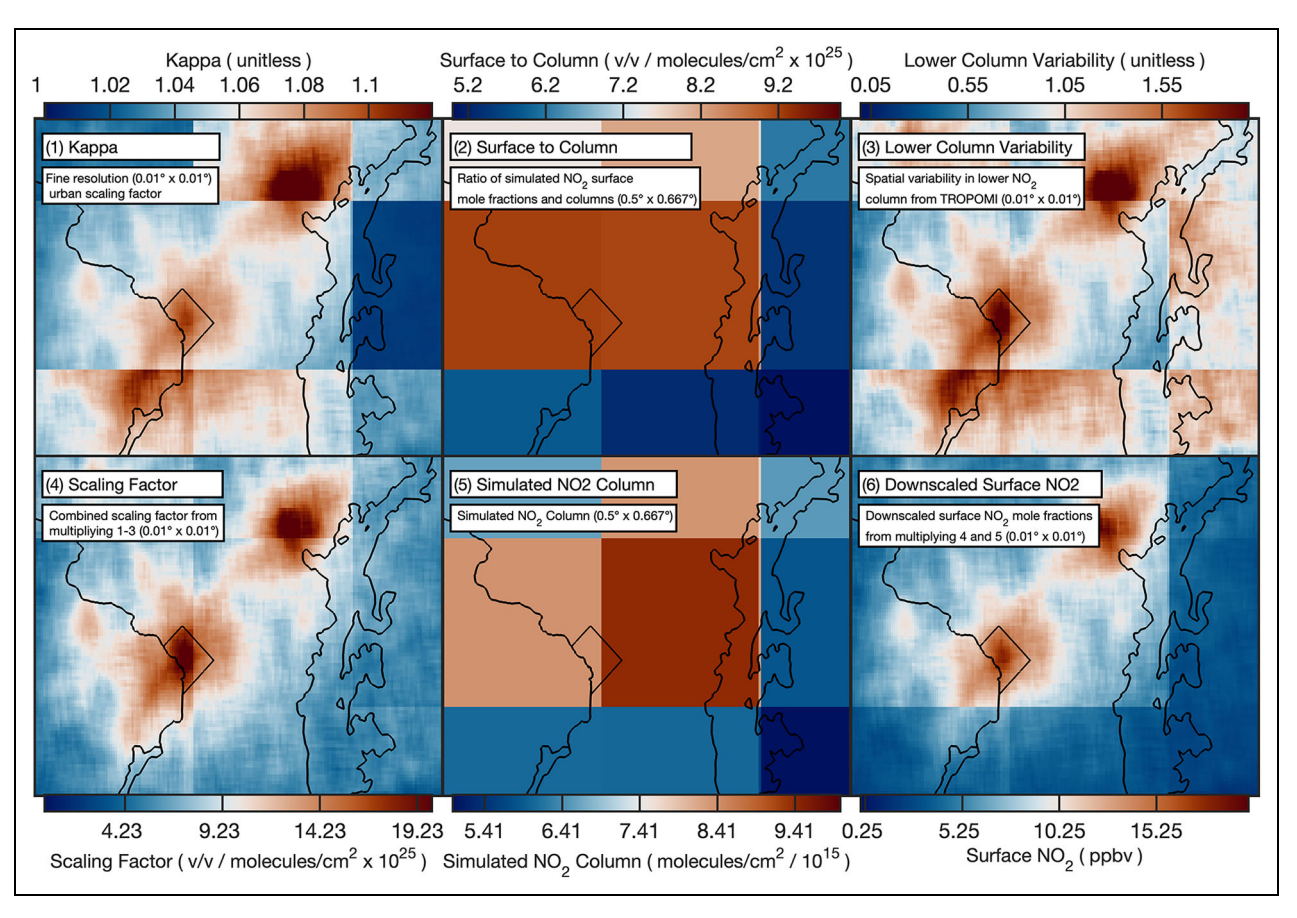


Figure 2. NO₂ **satellite downscaling method.** Illustration of the NO₂ downscaling procedure from Cooper et al. (2020) for estimating surface mole fractions from remote sensing observations of NO₂ columns, here modified for application to model simulated columns. DOI: https://doi.org/10.1525/elementa.2021.00043.f2

 $\frac{(v_i\Omega_I-\Omega_I^{\text{free troposphere}})}{(\Omega_I-\Omega_I^{\text{free troposphere}})}$, scaling factor (panel 4) is the 3 prior terms combined, simulated NO₂ column (panel 5) is Ω_I and the downscaled surface NO₂ (panel 6) is calculated by combining the scaling factor with the simulated NO₂ column.

These 3 cost functions, which we now refer to generically as J, are calculated using output from the forward model. Once the forward model simulation finishes and the cost functions are calculated, the adjoint simulation begins and calculates gradients of these cost functions with respect to emissions. The emissions we consider are BC, OC, NH₃, NO_x, SO₂, CO, and VOCs. We report only sizable sensitivities for each pollutant: For PM_{2.5}, we exclude direct emissions of CO; for O₃, we consider NO_x, VOCs, and CO; and for NO₂, we only consider NO_x. These gradients are calculated as:

$$\lambda_{I,k,d} = \nabla_{E_{I,k,d}} J = \frac{\partial J}{\partial E_{I,k,d}}.$$
 (4)

Here, $\lambda_{I,k,d}$ is the sensitivity or "gradient" of each of these cost function to their respective emissions parameters of species k at grid cell I on day d and $E_{I,k,d}$ refers to the emissions of species k at location I on day d.

These gradients are calculated at the model resolution $0.5^{\circ} \times 0.667^{\circ}$; but we consider them at the resolution of the NEI emissions $(0.1^{\circ} \times 0.1^{\circ})$ in order to better resolve contributions at finer resolutions. In doing so, we assume

that sensitivities at the coarse scale are constant, which fails to account for subgrid scale variabilities and introduces uncertainty. Ultimately, sensitivities are calculated at the coarse model resolution; however, we calculate contributions at the finer resolution of the NEI to improve the identification of regional and point sources to DC's pollution exposure.

For every grid cell, we multiply the sensitivity of the cost function to emissions from that grid cell of species k and day d with the NEI emissions in the same grid cell of the same species k, sector s, and the same day d. By multiplying these 2 quantities for every grid cell, we determine the unique contribution from emissions of a specific species, sector, and day to each of the 3 pollutant exposures:

$$dJ_{i,k,s,d} = (\lambda_{i,k,s,d} \times E_{i,k,s,d}). \tag{5}$$

Here, we refer to $dJ_{i,k,s,d}$ as the contribution to one of the pollutant exposure cost functions from emissions at location i, on day d of species k and of sector s. $E_{i,k,s,d}$ represents the NEI emission from grid cell i which we consider at daily, d, temporal resolution and are separated by species k and sector s. In the supplemental, we present the annual averaged adjoint sensitivities of all 6 anthropogenic precursor species of PM_{2.5} (BC, OC, NH₃, NO_x, SO₂, and VOCs) along with a time series of daily sensitivities for all species (S3). Sensitivities for O₃ and NO₂ are also

presented in the supplemental (S4 and S5). In all our results, we only present the contributions from anthropogenic emissions, as they are of most interest for air quality control policies, although contributions from natural sources are included in our modeling.

2.4. Health impacts

We calculate premature deaths from PM_{2.5} exposure following the methodology of the Global Burden of Disease (GBD) 2019 study (Murray et al., 2020) and calculate COPD premature deaths from O₃ exposure using a log-linear exposure response model (Jerrett et al., 2009). For PM_{2.5}, though the GBD 2019 methodology is currently the stateof-the-science technique, it generally estimates less premature deaths than another recently developed exposure response model, the Global Exposure Mortality Model (GEMM; Burnett et al., 2018). We consider the additional uncertainty introduced by the choice of concentrationresponse model in Section 3.5. The study used for the O₃ health impact assessment considers the relationship between 1-h max O₃ exposure and premature death and only considers respiratory death; however, a more recent study (Turner et al., 2016) relates the maximum daily 8-h average O₃ exposure to premature deaths and includes additional nonrespiratory causes that result in higher estimates of premature deaths. Pediatric asthma cases from NO₂ exposure are calculated using a log-linear exposure response model (Achakulwisut et al., 2019). All mortality rate and population data considered are exclusive to the federal district and do not include the surrounding metropolitan region. Age-stratified population data for DC during 2011 and 2016 are retrieved from the GBD Exchange Results tool for DC. Age-stratified mortality rates for DC for IHD, STROKE, COPD, LC, LRI, and T2D along with pediatric asthma incidence rates for DC during 2011 are retrieved from the GBD Exchange Results tool for DC (http://ghdx.healthdata.org/gbd-results-tool: accessed November 2020) for 2011. For 2016, pediatric asthma incidence rates are calculated using emergency department visits with a primary diagnosis of asthma from the DC Hospital Association compiled by the State Health Planning and Development Agency. We combine mortality or incidence rates and population estimates for DC with attributable fractions (AF) calculated as:

$$AF(z) = \frac{RR(z) - 1}{RR(z)}.$$
 (6)

Here, z is a pollutant exposure which can represent either the total exposure or this same total with the anthropogenic contribution, $dJ_{i,k,s,d}$ removed. In the latter case, we evaluate the AF of a case in which a specific anthropogenic contribution of unique location, species, sector, and day, is removed from the total exposure in DC. RR is the relative risk—the ratio of the risk of a health outcome occurring in an exposed population versus an unexposed population.

For PM_{2.5}, we estimate the age-specific relative risk for IHD, LC, STROKE, LRI, T2D, and COPD using the relative risk look-up tables from GBD 2019. These tables relate

exposure levels to relative risks for the aforementioned health impacts. Between exposure levels in these tables, we linearly interpolate relative risks. We calculate the relative risks for COPD from O₃ exposure using the log-linear exposure response model (Jerrett et al., 2009):

$$RR(z) = \exp^{\beta \Delta z},\tag{7}$$

where β is the concentration response factor that expresses the log slope of the relationship between risk of premature death and ozone exposure and Δz is the exposure with a counterfactual mole fraction removed. We use an estimated relative risk of death from COPD of 1.027 per 10 ppb O_3 mole fraction increment (Jerrett et al., 2009). We use a counterfactual O_3 mole fraction of 37.6 ppb in following with other studies (Cohen et al., 2017; Zhang et al., 2018).

For NO₂, we use the log-linear model (Achakulwisut et al., 2019) which takes the same form as Equation 7 with a relative risk of pediatric asthma cases of 1.26 per 10 ppb NO₂ mole fraction increment and a counterfactual NO₂ mole fraction of 2 ppb. Using this model, we calculate the relative risk for new pediatric asthma cases.

With the relative risks calculated, we can estimate the number of cases or the number of premature deaths from health outcome *O* as:

$$O = P \times BR_O \times AF(z). \tag{8}$$

The number of excess health outcomes O is equivalent to the product of the age-related population of the district, P (Murray et al., 2020), the baseline mortality or incidence rate of the same health outcome, BR_O (Murray et al., 2020), and the AF of exposure z as calculated by substituting the relative risks from Equation 7 into Equation 6 for O₃ and NO₂ and by using RR values from the look-up table for PM_{2.5}. The population and baseline rates are provided at the district level. The value z is the popweighted exposure of the district calculated following Equations 1–3. The AF is calculated twice for each grid cell, one time using the baseline pollutant exposure in DC, and another using that same baseline exposure with the source contribution removed. We take the difference between these attributable fractions multiplied by the population and baseline rate data to estimate the number of outcomes contributed by a specific source to health impacts in DC. By taking the difference in these 2 outcome estimates for every source category, we estimate the health impacts contributed by emissions for each grid cell. For all health impact analyses, we only consider the population living in the federal district, not the surrounding metropolitan area. Age-stratified population for 2011 and 2016 is provided in SI Table 1.

3. Results

3.1. Comparison to observations

We characterize the performance of the simulated concentrations from GEOS-Chem by comparison with in situ concentrations at 2 distinct timescales. First, we evaluate performance at the long-term timescales of pollutant exposure (**Table 2**) at which we calculate the adjoint cost functions, and second, we evaluate performance at the daily temporal resolution (**Figure 3**) at which we perform

Table 2. Simulated and in situ pollutant concentration comparison at exposure timescales. DOI: https://doi.org/10.1525/elementa.2021.00043.t2

	DC Measurement Location		
Pollutant	Hains Point Monitor (HP)	McMillan Monitor (MM)	River Terrace Monitor (RT)
Simulated annual PM _{2.5}	$14.0 \frac{ug}{m^3}$	$14.0 \frac{ug}{m^3}$	13.5 ^{ug} _{m³}
Satellite-corrected simulated annual PM _{2.5}	$13.4 \frac{ug}{m^3}$	$12.4 \frac{ug}{m^3}$	13.5 ^{ug} / _{m³}
Observed annual PM _{2.5}	$11.0 \frac{ug}{m^3}$	$11.2 \frac{ug}{m^3}$	$10.4 \frac{ug}{m^3}$
Simulated 6-month peak 1-h max O_3	72.2 ppbv	72.2 ppbv	N/A
Observed 6-month peak 1-h max O_3	57.7 ppbv	53.6 ppbv	N/A
Simulated annual NO ₂	7.7 ppbv	7.7 ppbv	N/A
Satellite-corrected simulated annual NO ₂	16.9 ppbv	16.6 ppbv	N/A
Observed annual NO ₂	14.6 ppbv	15.7 ppbv	N/A

Concentrations for all 3 pollutants ($PM_{2.5}$, O_3 , and NO_2) at 3 monitoring sites in DC: HP, MM, and RT. Simulated and observed values are available for all 3 pollutants; for $PM_{2.5}$ and NO_2 , the satellite-corrected simulated concentrations are included. Exposure timescales for $PM_{2.5}$ and NO_2 are annual averages; for O_3 , the exposure timescale is the 6-month peak period. For $PM_{2.5}$, concentrations were observed on 86, 347, and 344 days from HP, MM, and RT, respectively. For O_3 , mole fractions were observed on 356 and 363 days from HP and MM, respectively. For NO_2 , mole fractions were observed on 356 and 363 days from HP and MM, respectively.

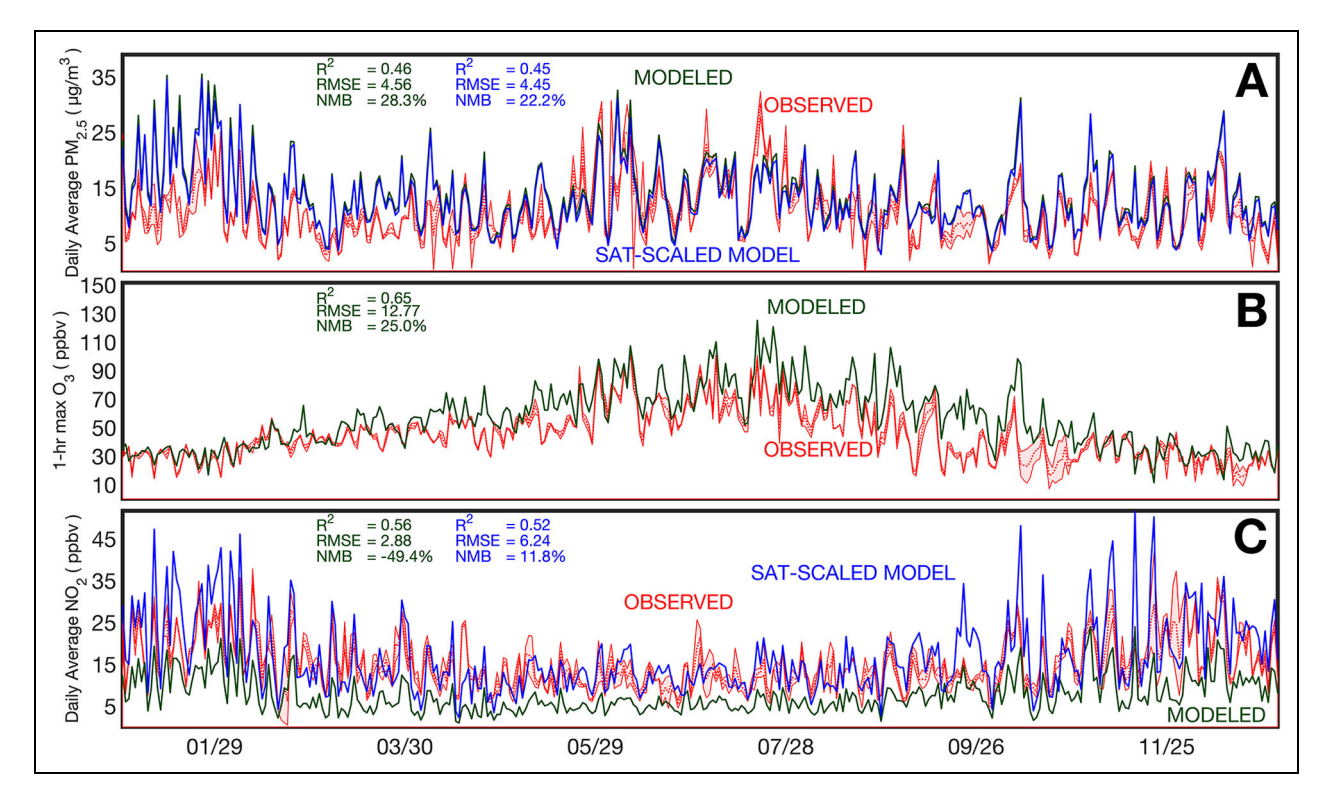


Figure 3. Simulated and in situ pollutant concentration comparison at the daily timescale. Comparison between simulated and observed concentrations of the 3 study pollutants: PM_{2.5} (A), O₃ (B), and NO₂ (C). Green indicates modeled concentrations; blue indicates satellite-corrected-simulated concentrations and red indicates observed concentrations. Monitoring data are averaged across all sites that recorded an observation for each day. Simulated and satellite-corrected values are taken for each site and then averaged across all sites. All data presented here are for 2011. Bias is modeled—observation. DOI: https://doi.org/10.1525/elementa.2021.00043.f3

our source attribution. By considering performance at these 2 distinct timescales, we characterize larger systemic biases in our model across longer periods and characterize uncertainty in the daily source attribution by considering the correlation between model simulated concentrations and observations. For PM_{2.5} and NO₂, we consider 24-h averaged daily, but for O₃, we consider the 1-h max value for each day, so that the comparisons between the simulated results and observations are consistent. The simulated concentrations of PM_{2.5}, O₃, and NO₂ have NMBs of +28.3%, +25.0%, and -49.4% when compared to the site-averaged annual average. Throughout the year, at the daily timescale, simulated concentrations of PM_{2.5}, O₃, and NO₂ have correlation coefficients of 0.46, 0.65, and 0.56, respectively, when compared to daily in situ observations indicating modest correlation at the daily timescale. For PM_{2.5} and NO₂, the exposure timescales are annual averages, and for O₃, it is the 6-month peak average. When satellite-derived data are used to scale simulated output, through rescaling for PM_{2.5} and downscaling for NO₂, biases decrease to +22.2% and +11.8%, respectively. When annual average remote-sensing-derived data are included in the adjoint cost function, the exposure and sensitivity calculations more accurately represent groundlevel in situ observations. This improvement in simulation accuracy is due to 2 distinct approaches: satellite "downscaling" and "rescaling." First, in downscaling, satellite-derived data account for variability at much finer resolutions than our model is capable of, allowing for the quantification of subgrid variability in simulated surfacelevel concentrations. This approach accounts for variability over 30 times finer for PM_{2.5} and over 3,000 times finer for NO₂ than the native model resolution. Second, in rescaling, between the forward and inverse simulation, simulated PM_{2.5} concentrations are scaled to the satellitederived concentrations averaged to the model resolution; this is not done for NO₂ as there is a discrepancy between the simulation year (2011) and the satellite-derived data years (2018–2019). This improvement specifically occurs in the cost functions, that is, the pollutant exposures; this approach does not improve the resolution of emissions in the model simulation.

Although both downscaling and rescaling contribute to improved performance across long-term timescales through reduction in biases, they have only minor effects on correlation since they are computed at the annual average timescale. Although not done here, the positive O_3 bias would be lowered if we compared mole fractions at 2 m as opposed to the first layer (approximately 65 m; Travis and Jacob, 2019) which we discuss in greater detail in Section 3.5. Overall, we calculate cost-function values of 12.4 $\frac{ug}{m^3}$, 74.5 ppbv, and 15.8 ppbv for $PM_{2.5}$, O_3 , and NO_2 , respectively.

3.2. Annual source attribution

We calculate emission contributions to pollutant exposures by considering distinct species and sector groups at a daily temporal resolution and at the $0.1^{\circ} \times 0.1^{\circ}$ spatial resolution of the NEI. These contributions are

aggregated across space into large regions, primarily states, and across time into a single end point while maintaining the species and sector groups. Through this aggregation, we identify the extent to which emissions from individual regions, sectors, and species contribute to adverse health impacts across a single year, 2011, in DC. We perform a source apportionment of pollution-related premature deaths from PM_{2.5} and O₃ exposure (Figure 4A) and perform a source apportionment of NO₂-related new pediatric asthma cases (Figure 4B). By performing source apportionments for health impacts, as opposed to concentrations, we simplify comparisons between individual pollutants and contextualize the impacts of emissions across all pollutants. To obtain a unified pollutant source apportionment, these health impacts could be further aggregated through an economic impact analysis; however, this is beyond the scope of this study.

3.2.1. Source contributions to pollution-related premature deaths

Anthropogenic emissions of pollutant precursor species contributed 263 (health impact assessment uncertainty: 130–444) pollution-related premature deaths to DC in 2011 (**Figure 4A**) or 5% (2–7) of all deaths in DC in 2011. Of these pollution-related premature deaths, PM_{2.5} exposure accounted for 9.4 times more premature deaths than O₃, even though the attainment status of PM_{2.5} is in better compliance with the NAAQS than O₃ in the DC–MD–VA nonattainment area. Because of this, the sources of pollution-related premature deaths more closely resemble the sources of PM_{2.5} exposure than O₃ exposure. Source apportionments for all 3 individual pollutant exposures are available in the supplemental (S6–S8).

The sectoral sources of pollution-related premature deaths were relatively diverse, with 7 of the 10 sectors considered contributing 5% or more of the premature deaths in DC. Emissions from the surface sector contributed to premature deaths primarily through PM_{2.5}-related premature deaths (94%) rather than O₃-related premature deaths. From the surface sector, emissions of OC, VOCs, and NO_x were the highest contributors making up 36%, 31%, and 14%, respectively, of all surface contributions. Surface emissions come from a wide variety of subsectors (S1) with the ones that contributed the most from these species being solvent use, gas stations, residential nonwood combustion, industrial combustion, and locomotives.

On-road vehicle emissions contributed 23% of all pollution-related premature deaths. This large contribution is consistent with expectations as the mid-Atlantic region has high-traffic volumes. A majority of on-road vehicle emission contributions to pollution-related premature deaths were from contributions to $PM_{2.5}$ exposure (82%) rather than O_3 exposure (18%); however, O_3 -related premature deaths were proportionally higher than for other sectoral contributions to pollution-related premature death. This is due to the strong sensitivity of O_3 exposure to NO_x which, across both pollutants, made up 42% of on-road contributions to pollution-related premature deaths. Following NO_x , on-road vehicle emissions contributions from VOCs (27%) and primary

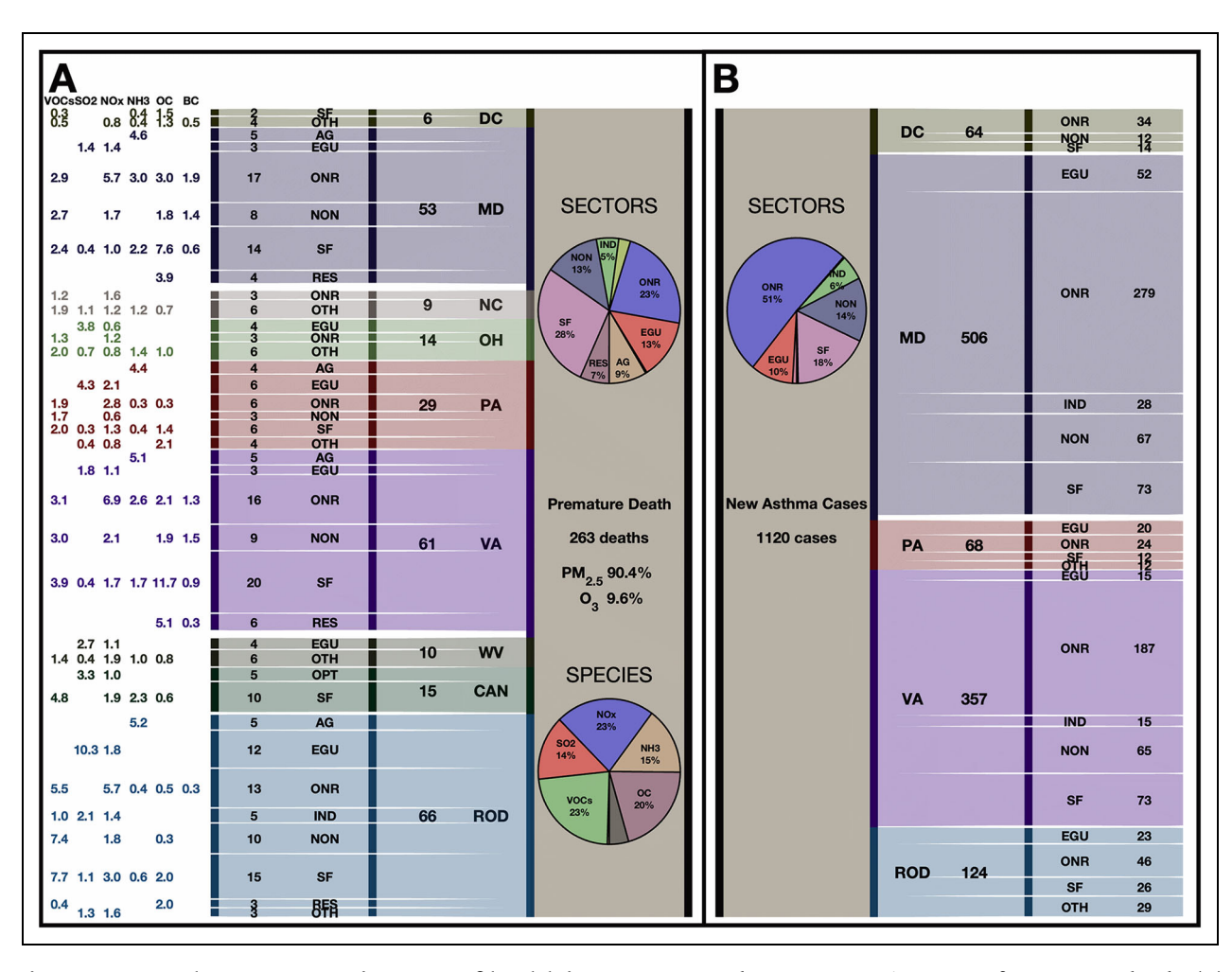


Figure 4. Annual source apportionment of health impacts. Annual source apportionment of premature deaths (A) and asthma incidence (B). Pie charts indicate total sectoral and species apportioning across the entire domain and time period. In the pie charts, values below 5% are not labeled. The columns indicate state apportioning, sectoral apportioning of each state, and species contributions to each sector state combination. All locations within the domain that are not considered in this figure are lumped into the rest-of-domain region; these are locations that contributed less than 6 premature deaths and 30 new asthma cases. For the state-level breakdowns, all sectors that have small contributions are combined into an "OTH" category; the pie charts, representing the sectoral breakdowns across the domain, do not have an "OTH" category. DOI: https://doi.org/10.1525/elementa.2021.00043.f4

carbonaceous aerosols (18%) were the largest. Contributions from on-road vehicle emissions primarily came from DC and its surrounding area (MD, VA, and PA) for both PM_{2.5} (66%) and O₃ (72%). This is due to 2 reasons: on-road vehicle emissions from DC and its surrounding area are high, making up 8.2% of total on-road vehicle NEI emissions in 2011 as implemented in GEOS-Chem, and locations further away from DC are more likely to have very small or negative NO_x sensitivities.

In 2011, large EGU emission contributions to pollution-related premature deaths in DC came from a wide spatial range spanning from southern Maryland to the Ohio River Valley. Post 2011, however, EGU closures resulted in decreased contributions as discussed in Section 3.4. EGU contributions to air-pollution-related premature deaths were almost exclusively of SO_2 (72%) and NO_x (24%). EGU emissions from distant states contributed proportionally more than other sectors; 63% of all EGU contributions came from states beyond DC and its surrounding area

with major contributions from Ohio River Valley states like Ohio (13%), West Virginia (11%), Kentucky (5%), and Indiana (5%).

Across all sectors, local and regional emissions (DC, MD, VA, and PA) unsurprisingly contributed the most (57%) to pollution-related premature death. NO_x concentrations in rural areas are generally biased low due to the overactive conversion of NO₂ to terminal sinks of O_x like HNO₃ (Canty et al., 2015; Goldberg et al., 2016; Travis et al., 2016) in many chemical transport models including GEOS-Chem. This could result in an over attribution of O₃ to local sources. Beyond local and regional contributions, long-range emissions from further away states like Michigan, North Carolina, West Virginia, and Ohio contributed 14% to DCs pollution-related premature deaths. Considering the highest sectoral contributors on a state-by-state basis is useful for developing targeted emissions mitigation policies. In Maryland and Virginia, the 2 largest contributing states, on-road vehicle, and surface emissions contributed the most to pollution-related premature deaths; this is consistent with the domain-wide sectoral breakdown. Some states, however, exhibit divergent sectoral breakdowns. In Pennsylvania, the third highest contributing state, contributions were more evenly distributed across EGU, on-road vehicle, surface, and agricultural emissions. Regional patterns in the chemical species of contributions are more difficult to interpret than sectors. Regional variability in contributions is more closely linked to sectors than chemical species; for example, where there are more on-road emissions, there will generally be more NO_x emission contributions, and where there are more EGU emissions, there will generally be more SO₂ emission contributions. While our methodology allows us to identify such regional species relationships (S13), we focus primarily on the sectoral relationships here.

3.2.2. Source contributions to NO_2 -attributable pediatric asthma cases

Next, we consider the source contribution to NO_2 -attributable pediatric asthma cases (**Figure 4B**). Anthropogenic emissions of NO_x were responsible for 1,120 (391–1,795) new pediatric asthma cases in DC for 2011 or 32% of all new pediatric asthma cases. We note the persistence of these NO_2 -related health impacts despite attainment of both the 1971 annual mean and 2010 1-hr max NAAQS in the DC–MD–VA region.

Two factors drive the sectoral contribution to pediatric asthma cases in our analysis: the exclusive NO_x sensitivity and the strong local signal due to the short lifetime of NO₂. Chemical transport models generally underestimate the recycling of NO2 leading to shorter effective lifetimes (Canty et al., 2015; Romer Present et al., 2020) which could enhance the local signal in our analysis. Because of this, sectors with the most NO_x emissions and sectors that have proportionally higher emissions in DC and the surrounding area contribute the most to new pediatric asthma cases. One sector that has both of these qualities is the on-road sector which contributes a majority of the NO₂-attributable asthma case in DC; 92% of contributions from this sector come from local and regional sources (DC-MD-VA-PA). The next 3 largest sectors, surface, nonroad and EGU, all have large local and regional contributions of 87%, 94%, and 79%, respectively. The EGU sector has the smallest local and regional contribution of these sectors due to distant contributions from Ohio River Valley states ranging from 2% to 6% per state. The short lifetime of NO₂ is most apparent when considering total state contributions. Maryland and Virginia combined makeup 77% of asthma contributions followed by Pennsylvania (6%) and DC (6%). The contributions of emissions from other, more distant, states are much smaller for NO₂attributable new asthma cases than for PM_{2.5}- and O₃attributable premature deaths.

3.2.3. Spatial distribution of source contributions

Here, we focus on quantifying the role of local versus regional versus distant contributions to pollutant exposures in DC. Denoting the center of DC as 38.9°N, 77.0°W, in this section, we consider "local" contributions

as coming from emissions from grid cells with centroids within 0.5° latitude and longitude of the center of DC. We consider "regional" contributions as those coming from within 2.0° latitude and longitude of the center of DC. We consider "distant" contributions as those coming from beyond 15° latitude and longitude of the center of DC. We use the term "extra-regional" to refer to all emissions outside of the "regional" area including "distant" emissions. We also identify contributions from specific distant point sources and sectors.

Previously, we considered the spatial distribution of contributions in terms of adjoint sensitivities calculated at the resolution of model grid cells ($0.5^{\circ} \times 0.667^{\circ}$) aggregated up to the state level. Here, we further improve the resolution of these spatial contributions by putting the model sensitivities on the fine resolution (0.1 $^{\circ}$ × 0.1 $^{\circ}$) grid of the NEI as implemented in GEOS-Chem. In doing so, we assume that there is no subgrid variability in the sensitivities and that sensitivities remain constant at this fine resolution across the larger model grid cells. This assumption introduces error in our analysis. At this finer resolution, there would naturally be areas of higher and lower sensitivity. Influences from topography, proximity to DC, and meteorological factors, which all vary at this fine resolution, could impact whether a pollutant exposure would be more or less sensitive to emissions from a fine grid cell. Despite these limitations, a benefit of this approach is that contributions from individual point sources, road systems, and smaller regions of states are identifiable (**Figure 5**). Because of this, we will consider emission contributions at the fine resolution of the NEI (0.1 $^{\circ}$ \times 0.1 $^{\circ}$). The spatial distribution of sectoral contributions is discussed in this section, and the spatial distribution of species contributions is presented in the supplemental (S13). We mark the prominent locations discussed in this and the following sections in the supplemental (S16) and recommend referring to this when specific locations in the area surrounding DC are discussed.

Some spatial emission contribution patterns occur similarly for all 3 pollutant exposures. Emissions from within and directly surrounding DC contribute the most to all pollutant exposures. Local emissions, as described above, contribute 29%, 34%, and 69% of PM_{2.5}, O₃, and NO₂ exposures, respectively. These 100 grid cells represent only 0.03% of the total area of the NEI. Local emissions contribute over twice as much to NO₂ exposure than the other 2 pollutants which is consistent with the shorter lifetime of NO₂ as discussed previously. Another common feature across all 3 pollutants is large emission contributions from 2 highways, 195 and 181. Additionally, emissions from point sources, primarily from EGUs, in western Pennsylvania and along the border of Ohio and West Virginia contribute to all 3 pollutants with varying magnitudes.

Although both regional and distant emissions contribute to DC's PM_{2.5} exposure, 53% of DC's PM_{2.5} exposure is contributed by regional emissions as defined above. Emissions from Richmond, VA (37.5°N, 77.4°W) and the surrounding area (0.3° around this point), which we consider as "regional," contribute 1.8% of all PM_{2.5} exposure in DC. A few notable sites fall outside of the "regional" domain.

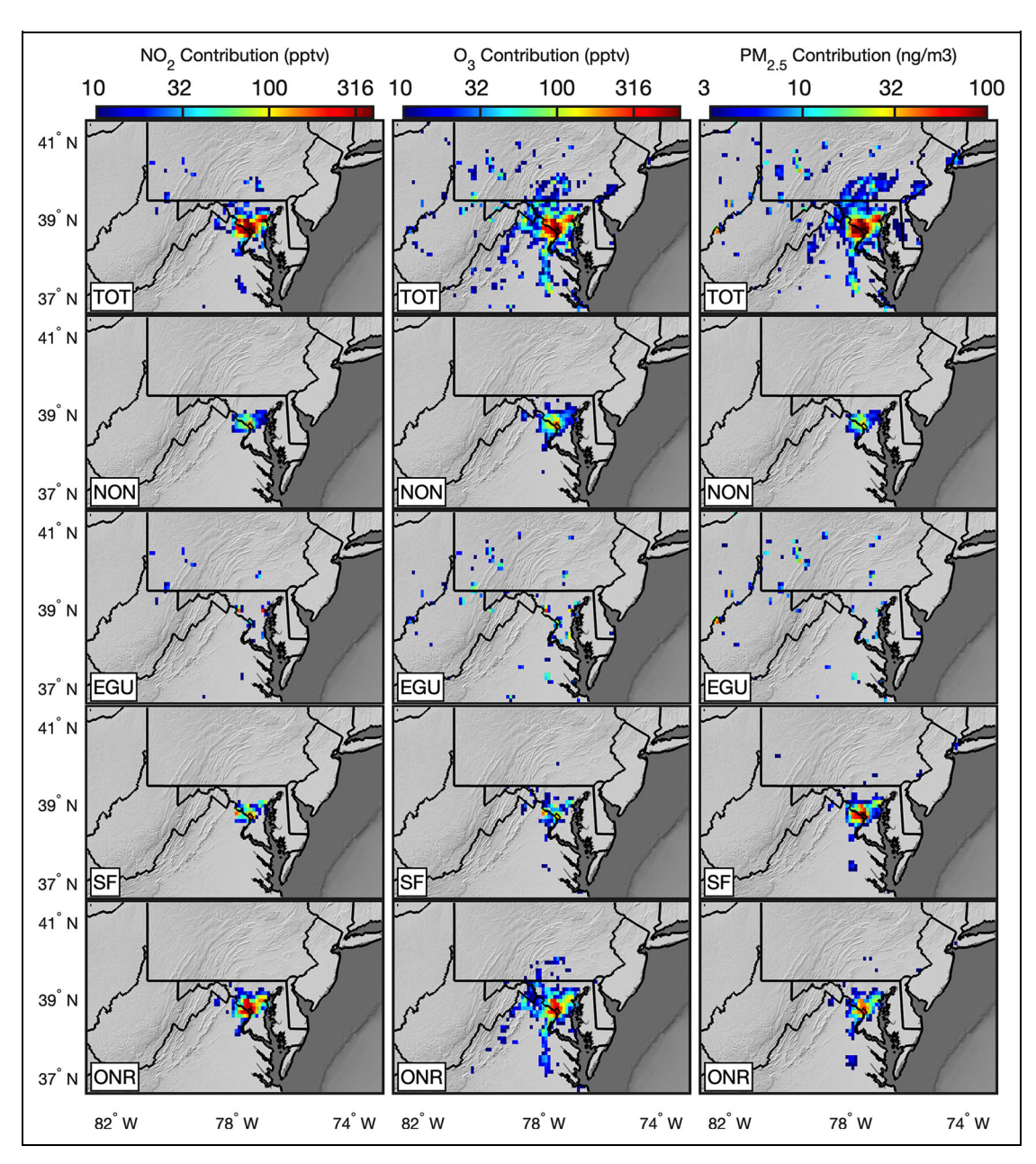


Figure 5. Gridded contributions to the 3 pollutant exposures. The spatial distribution of annual contributions of emissions to exposures of PM_{2.5}, O₃, and NO₂. Grid cells where emissions contributed less than 10 pptv, 10 pptv, and 3 ng/m³ to DC's annual exposures to PM_{2.5}, O₃, and NO₂, respectively, are not shown. Total (TOT) contributions for each pollutant are given in the first row; subsequent rows show the spatial distribution of contributions from the 4 highest contributing sectors: nonroad (NON), energy-generation units (EGU), surface (SF), and on-road (ONR). DOI: https://doi.org/10.1525/elementa.2021.00043.f5

Emissions from New York City (40.7° N, 74° W) and the surrounding area (0.3° around this point) contributed 0.8% of DC's PM_{2.5} exposure. Although it was decommissioned in 2018, in 2011, emissions from the Inco Superstack in Sudbury, Ontario (46.4° N, 81.2° W), contributed 0.3% of all anthropogenic PM_{2.5} exposure in DC.

Regional emissions contribute 59% of O_3 exposure, proportionally more than their contributions to $PM_{2.5}$ exposure. This is partially due to above average NO_x emissions in the region surrounding DC to which O_3 is more sensitive to than $PM_{2.5}$. O_3 exposure has a larger contribution from "distant" emissions, as described above, with

this category making up 6.7% of O_3 contributions compared to 5.8% of $PM_{2.5}$ and 0.4% of NO_2 . Emissions from Richmond, VA, contributed 2.4% of the anthropogenic contribution to O_3 exposure.

A cluster of power plants within 0.3° of Morgantown, WV (39.6°N, 80.0°W), with the largest emissions coming from 3 EGUs (Hatfield's Ferry Power Station, Fort Martin Power Station, and Longview Power) contribute proportionally more to O_3 exposure (1.1%) than to $PM_{2.5}$ exposure (0.6%). At the same time, power plants near Parkersburg, WV (39.3°N, 81.6°W), with the largest emissions coming from 2 EGUs (Muskingum River and

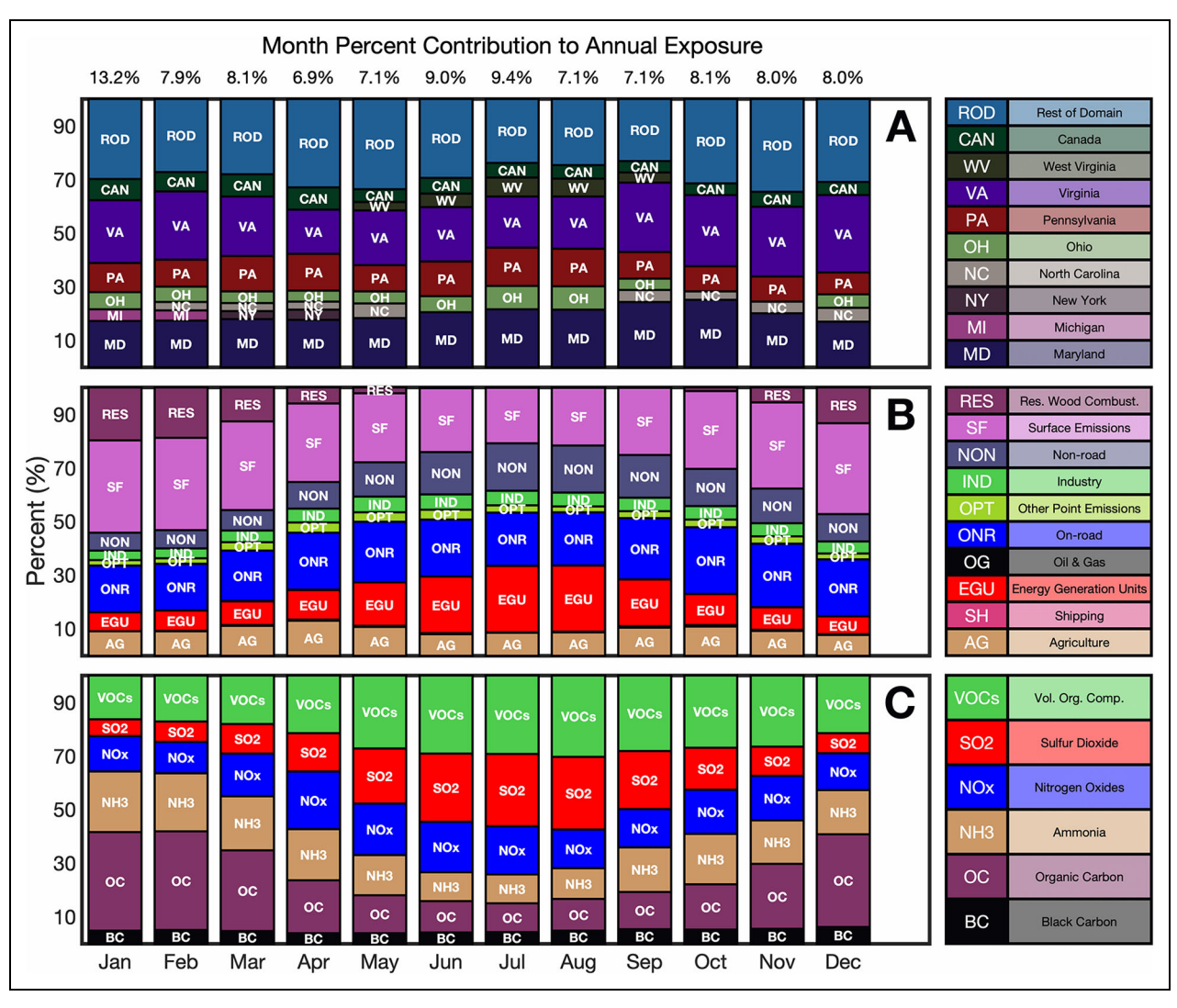


Figure 6. Seasonal variations in PM_{2.5} sources. Normalized monthly PM_{2.5} contributions from regions (A), sectors (B), and species (C). Percentage of total annual contribution for each month is given above each column. Labels for regions, sectors, and species are given to the right of the normalized plots. Regions that contribute less than 3% to a given month are grouped into the rest-of-domain category. All sectors and species are included for each month; however, sectors that contributed less than 2% to a month are not labeled for that given month. DOI: https://doi.org/10.1525/elementa.2021.00043.f6

Pleasants Power Station), contribute more to $PM_{2.5}$ exposure (0.5%) than to O_3 exposure (0.3%) in DC. These differences are initially somewhat counterintuitive as we expect that transport would be one of the strongest drivers for extra-regional contributions which would be constant across pollutants. This difference, however, can be explained by the speciation of emissions. The sites around Morgantown emitted 50.9 Gg of NO_x and 17.6 Gg of SO_2 in 2011, while the sites around Parkersburg emitted 6.8 Gg of NO_x and 56.1 Gg of SO_2 in 2011. Despite its further distance, the higher SO_2 emissions of the sites near Parkersburg lead to higher $PM_{2.5}$ exposure contributions in DC.

3.3. Pollutant exposure contributions at finer temporal scales

At annual timescales, on-road vehicle NO_x emissions, primarily from DC and its surrounding area, contribute the

most to DC's air pollution and its associated health impacts. However, decomposing this source attribution temporally to individual months and subsequently including seasonal changes reveals the complexity inherent to source attribution. Policies that consider this added complexity can increase their effectiveness beyond decisions made solely based on annual source apportionment, which may fail to completely characterize dynamic monthly changes in emissions and meteorology. In the following analysis, we consider seasonal changes in meteorology, transport, and atmospheric chemistry—contained within the daily sensitivities—along with seasonal changes of the magnitude of emissions from daily NEI emissions to characterize the overall seasonality of source contributions across regions, sectors, and species (**Figures 6** and **7**).

During the summertime in the eastern United States, the jet stream weakens and shifts northward yielding meteorological conditions that are more conducive for

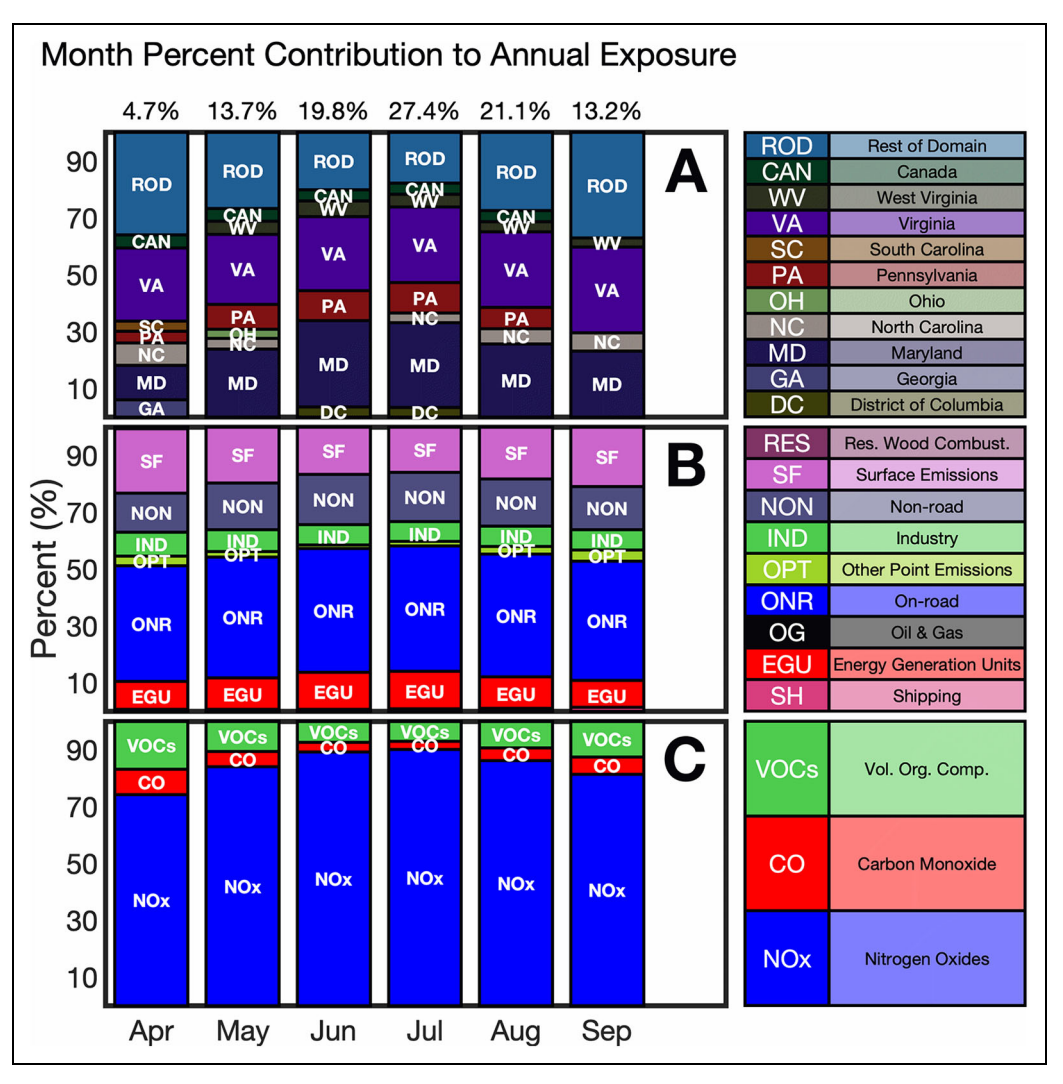


Figure 7. Seasonal variation in O₃ sources. Normalized monthly O₃ contributions from regions (A), sectors (B), and species (C). Percentage of total annual contribution for each month is given above each column. Labels for regions, sectors, and species are given to the right of the normalized plots. Regions that contribute less than 3% to a given month are grouped into the rest-of-domain category. All sectors and species are included for each month; however, sectors that contributed less than 2% to a month are not labeled for that given month. DOI: https://doi.org/10.1525/elementa.2021.00043.f7

O₃ formation (Kousky and Ropelewski, 1997). During this time, OA formation from emitted VOCs and sulfate formation from emitted SO₂ may be more favorable due to more active photochemistry (Kim et al., 2015). In the wintertime, colder and wetter conditions are more favorable for emitted NH3 to form ammonium nitrate and less favorable for O₃ formation due to a reduced photochemical source (Zhang et al., 2015). Our simulation captures this seasonality in composition; sulfate and SOA concentrations are 19% and 41% higher in the summertime than in the wintertime while ammonium nitrate is 126% higher in the wintertime than in the summertime. Beyond meteorological seasonality, there is seasonality to anthropogenic emission behaviors; higher temperatures in the summer lead to an increased demand for air conditioning and subsequently more EGU emissions. In the wintertime, cooler temperatures prompt increased residential natural gas and wood combustion. There is also inherent seasonality to natural emissions, for example, biogenic emissions are higher in the summertime in the eastern United States prompting more SOA formation. We present the seasonal source apportionment in terms of exposures, as opposed to health impacts, to characterize seasonal contribution differences across pollutants.

3.3.1. Seasonal PM_{2.5} source apportionment

We present normalized monthly emission contributions to PM_{2.5} exposure separated into the 3 previously considered source groups of regions, sectors, and species (**Figure 6**).

Normalization for each month is done by dividing each source category contribution by the total anthropogenic contribution from the month. Sectoral contributions have among the strongest seasonality for $PM_{2.5}$. RES wood combustion emissions contribute 70.1 times more in the wintertime, defined to be December through March, than in the summertime, defined to be May through August; this is unsurprising as more residential wood combustion occurs in the winter. In contrast, in the summer, EGU

emissions contribute 159% more than in the winter which corresponds with increased energy demand from heavier AC usage. Surface sector emissions peak in the wintertime with 71% larger contributions than in the summertime; the above average wintertime contributions come primarily from emissions of OC, NH₃, and VOCs which, at annual time scales, are mostly associated with waste disposal, industrial combustion, and solvent use (S1). Nonroad vehicle emission contributions are 99% higher in the summertime than in the wintertime. This contribution peak corresponds with national emission increases of 60%, 83%, and 61% from the 3 most emitted species from the nonroad sector, VOCs, NOx, and OC. Adjoint sensitivities calculated for these 3 species are 17%, 121%, and 3% higher in the wintertime than in the summer indicating that this higher summertime nonroad contribution persists despite unfavorable formation conditions. Agricultural, industrial, and on-road contributions remain relatively constant throughout the year with summer contributions -19%, +21%, and -2% the winter values. The latter 2 are not surprising as these sectors emission patterns remain relatively stable throughout the year; however, we would expect agricultural contributions to share a somewhat similar seasonality with NH₃ contributions. This difference in seasonality is explained by emission patterns. During the summertime, agricultural emissions contribute 75% of all NH₃ contributions, while in the wintertime, agricultural contributions dip making up only 46% of NH₃ contributions. In contrast, NH₃ sensitivities in the wintertime are 300% larger than in the summertime. This suggests that increased agricultural emissions in the summertime are mitigated to some extent by less favorable PM_{2.5} formation conditions, resulting in relatively consistent agricultural contributions year-round.

Of all the source categories, regionality has the weakest relationship to seasonality. Across all months, emissions from local and regional sources (DC, MD, PA, and VA) contribute the largest portion of anthropogenic PM_{2.5} exposure in DC; the local contribution from emissions in each month ranges from 46% in April to 69% in September. For every month, the 3 largest regional contributors are Virginia, Maryland, and Pennsylvania, albeit in varying order. In the wintertime, high contributing colder states at more northerly latitudes (PA, OH, MI, IN, IL, and NY) contribute 14% more to PM_{2.5} exposure than in the summertime, due to higher residential contributions from this region across this period. Considering the EGU sector, the high contributing Ohio River Valley States (PA, OH, WV, IN, and KY) contribute 14% more in the summertime, when there is an increased demand for energy, than in the wintertime. As some states fall in both groups, this summertime-wintertime difference is less pronounced than when considering sectoral seasonality exclusively from regionality as considered previously. Even though local and regional emissions contribute the most throughout the year, one interesting feature of the regional seasonality is the increased contribution from emissions from distant locations, defined to be all states excluding the nearby states (DC, MD, PA, VA, OH, MI, IN, IL, WV, KY, TN, NC, and NJ), in the wintertime. These distant states contribute 34%

more in the wintertime than in the summertime owing to stronger wintertime westerlies and longer chemical lifetimes of many species owing to reduced photochemical and physical sinks.

Species emission contributions also have strong seasonal patterns for PM_{2.5} exposure. All species except BC and NO_x have large differences in contributions between summer and winter. Emissions of SO2 and VOCs contribute more in the summertime with 171% and 47% larger contributions; this is consistent with seasonal patterns of PM_{2.5} composition in the southeastern United States (Kim et al., 2015) as in the summertime there is increased photochemistry driving the oxidation chemistry needed for the formation of sulfate and SOA. On the other hand, emissions of NH3 and OC contribute more in the wintertime with 105% and 236% larger contributions. For NH₃, as discussed previously, there are higher wintertime sensitivities due to more favorable formation conditions of ammonium nitrate (Guo et al., 2019). Emissions of OC contribute more in the winter for a different reason, as sensitivities are only 17% higher in the wintertime. For OC, the increased residential emissions during the wintertime, transitioning from 1.6% of OC contributions in the summertime to 41% of OC contributions in the wintertime, are responsible for the large seasonal differences. Overall, our methodology allows us to disentangle the relationships between regions, sectors, and species to accurately identify the driving forces for seasonal changes in contribution.

3.3.2. Seasonal O₃ source apportionment

We characterize seasonality in this discussion by comparing emission contributions from the middle of the period, or the summertime peak (June, July) to the shoulder season (April, September). There were small emissions contributions from March; however, they were in total less than 0.1% and thus are excluded from this discussion. Local and regional emissions (DC-MD-VA-PA) contribute 71% and 70% of O₃ exposure contributions in June and July; however, they only contribute 43% and 58% of O_3 exposure contributions in April and September. This is consistent with expectations; during the middle of summer, there is a larger photochemical sink than during the shoulder season which shortens the lifetime of many chemical species. Emissions from the Ohio River Valley states contributed 5.5 times more in the middle of the period than at the ends of it, making up 9% of contributions at the ends of the period compared to 21% of contributions in the middle of summer; this corresponds to increased EGU demand and emissions. While summertime NO_x sensitivities were 27% higher in the peak than in the shoulders, the more favorable O₃ formation conditions in the peak are not nearly strong enough to fully explain the shift in contributions.

Sectoral seasonality of contributions to O_3 exposure was, generally, less pronounced than regional seasonality. In the middle of summer, emissions from on-road vehicles, nonroad vehicles, and EGUs contributed 44%, 15%, and 9% of all contributions compared to 41%, 18%, and 13% during the shoulder season. Surface emissions were

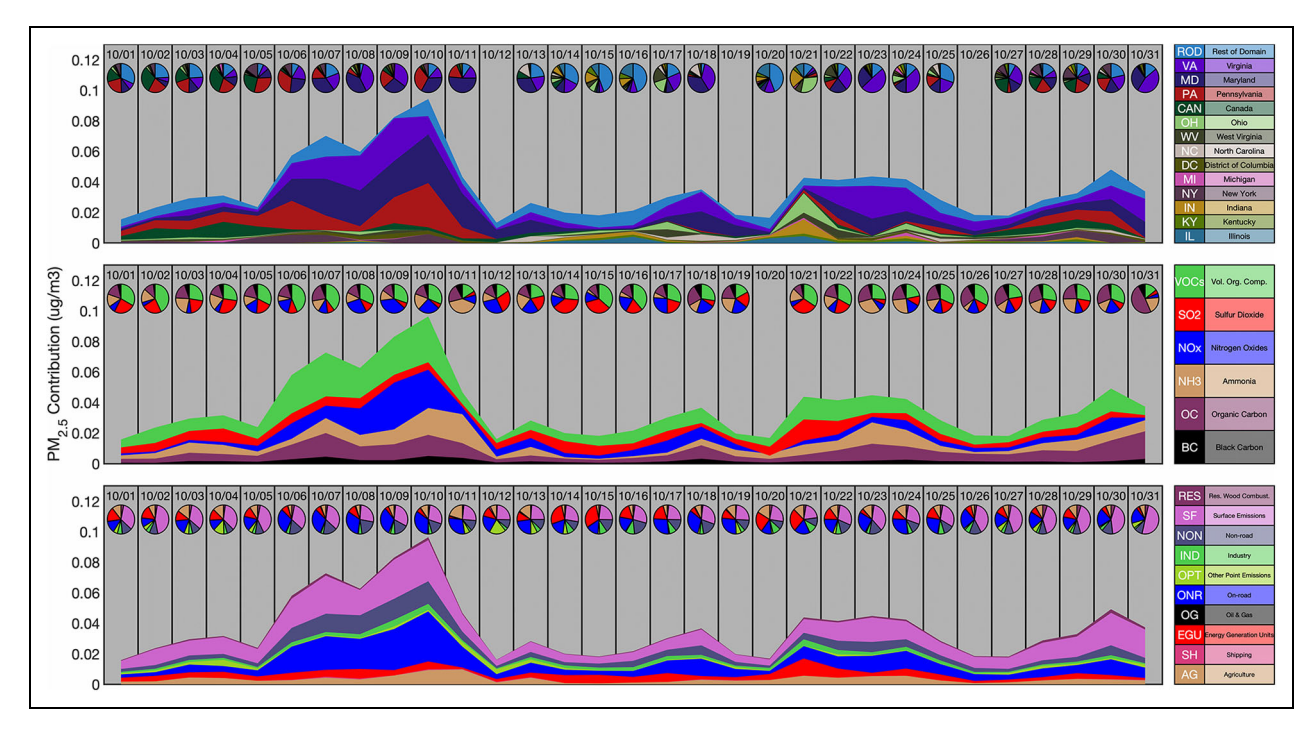


Figure 8. Daily contributions to PM_{2.5} exposure in October. Daily emission contributions to PM_{2.5} exposure in October separated by region, species, and sector. The area plot shows the absolute amount contributed by different source categories for each day. Vertical black lines block out contributions from specific days; for most days, a pie chart is included that shows the relative breakdown of sources for the specific category. Pie charts are excluded for days when at least one source category had a negative contribution. The 13 highest contributing regions are presented; all other regions are grouped into the "rest-of-domain" category. All sectoral and species contributions are included. DOI: https://doi.org/10.1525/elementa.2021.00043.f8

the only source to exhibit a decrease during the middle of summer. During the shoulder season, surface emissions contribute 22% of all O_3 exposure contributions; however, during the middle of summer, they only contribute 17%. Despite this, surface emissions still contribute 100% more O_3 exposure contributions in the middle of summer than in the shoulder season; this indicates that the proportional surface contribution decrease in the peak of summer is more a product of other sectors having larger proportional increases than changes to emission patterns or sensitivities.

Finally, considering species seasonality, contributions from emissions of VOCs and CO make up their largest proportional contributions in the shoulder season; they contribute 16% and 8% compared to 8% and 3% during the middle of summer. During the middle of summer, there is a greater availability of nonanthropogenic VOCs, from biogenic emissions that contribute to O_3 formation. As a result, more O_3 is formed overall but proportionally less is contributed by anthropogenic VOCs. NO_x contributions have the opposite seasonal pattern of VOCs and CO proportionally peaking at 89% in the middle of summer compared to 75% during the shoulder season. During the peak of summer, more active photochemistry causes quicker NO_x cycling and in turn more formation of O₃ corresponding with the modeled summertime NO_x contribution peak. Beyond this, seasonal patterns in nonroad and on-road emissions contribute to higher NO_x contributions in the middle of summer. We do not include normalized NO_2 monthly source apportionment in this discussion as the seasonality of NO_2 is even less pronounced than O_3 ; however, a similar figure can be found in the supplemental (S9).

3.3.3. Daily emission contributions to pollutant exposures

As presented above, disaggregating annual source apportionments to the monthly timescale improves characterization of the sources of pollution in DC through the consideration of seasonality; however, short-term dynamic changes of the factors involved in pollutant formation like a shift in the average advection direction, a period of sustained higher or lower temperatures, a high precipitation period, or a unique emission event are not considered when source apportionments are performed at the monthly level. In this section, we present daily contributions, considering how emissions from a single day contribute to pollutant exposures, for PM_{2.5} exposure, while still maintaining the source categories of regions, sectors, and species. We present an example of these daily source contributions (**Figure 8**) for PM_{2.5} exposure for the month of October; in this month, a unique emission event occurs with a proportionally large annual contribution. Daily contributions for all available months across all 3 pollutants are presented in the supplemental (S10-S12). Although we briefly discuss O₃ and NO₂ daily contributions here,

most of the discussion of daily emission contributions to O_3 and NO_2 exposure are included in the supplemental.

Overall, for longer lived species with more diverse sources, like $PM_{2.5}$ and O_3 , a daily source apportionment approach captures unique events by identifying both the sources of emissions and the magnitude of their contributions over some period of time. This approach simultaneously quantifies how emissions from a day or period contribute to a pollutant exposure and where those contributions came from. However, the daily source apportionment approach is less beneficial for shorter lived species, like NO_2 , as there is little daily variation in sources.

For daily variability in pollutant contributions, it is useful to quantify daily variability in emissions as well to identify whether emission patterns or adjoint sensitivities are the major driver for variability for a given pollutant and species. For PM_{2.5} precursor species, consider the emission variability for BC (73%–117%), OC (74%–125%), NH₃ (63%–194%), NO_x (85%–110%), SO₂ (78%–122%), and VOCs (87%–125%) where ranges indicate the ratio of the least and most emission from a single day to the mean value of the month.

We consider how daily emissions from October (Figure **8**) contribute to DC's annual PM_{2.5} exposure. The most notable feature in October was a period of increased emission contributions between October 6 and 10; PM_{2.5} precursor emissions during this 5-day event contributed 0.4 ug/m³ or 2.6% of all anthropogenic contributions to annual PM_{2.5} exposure in DC. On average, emissions during this period contributed 1.9 (1.5-2.5) times the average daily contribution in 2011. Across this 5-day period, emissions from Maryland (32%), Virginia (23%), Pennsylvania (21%), and New York (5%) made up most of the contributions. Although emissions from New York were relatively small in magnitude, proportionally they were higher than average; emissions contributed 4.7 times more, as a daily average, compared to the rest of the year and emissions during this 5-day period alone contributed 6% of all of New York's emission contributions to DC's PM_{2.5} exposure. Across all states, over this 5-day event, on-road vehicle (32%), surface (30%), nonroad (17%), and agricultural (7%) emissions that originated from VOCs (34%), NO_x (25%), OC (16%), and NH₃ (13%) contributed the most to PM_{2.5} exposure in DC. Most notably, during this event, on-road vehicle emissions and NO_x emissions contributed proportionally more than during the rest of the month when these emissions contributed 25% and 17%,

Across this period, and throughout most of the year, the variability in adjoint sensitivities, which include meteorological variability, contributed more to the daily variability in source contributions than day-to-day variability in the emissions themselves. Daily contributions to PM_{2.5} exposure have sizable differences from the monthly mean contributions; they vary from 28% to 284% of the monthly mean value. Comparing this variability to emissions variability, we find that most of the day-to-day variability is explained by meteorology, characterized by the adjoint sensitivities, and not from the emissions. This is

also true for the other 2 pollutants, as discussed in the supplemental.

3.4. Exposure contribution changes between 2011 and 2016

In this analysis, we consider the changes in exposure associated with changes to emissions between 2011 and 2016 (**Figure 9A**), quantifying how decreases in specific aerosol and ozone precursor emissions resulted in substantial health benefits of reduced premature deaths and new pediatric asthma cases. As the changes in emissions from 2011 to 2016 are smaller than the 100% changes considered for the source attribution of 2011 presented above, the results in this section are more accurately captured by our linear response estimates as discussed in Section 3.5. We combine sensitivities calculated using 2011 meteorology with emissions from 2016 to estimate the contribution of emissions to pollutant exposures; this allows us to assess the impact of emission changes without considering changes in meteorology.

For the source attribution of changes in both premature deaths and new asthma cases, we forego discussion of the surface, oil and gas, and industry sectors due to differing sectoral definitions between the NEI 2011 and NEI 2016. We do compare changes in EGU and other-point contributions with an important caveat; due to changes in methodology of the NEI, there are components of both the EGU and other-point sectors, as defined in the NEI 2016, that are in the surface sector. Any comparisons of these sectors between 2011 and 2016 can be considered as lower bound estimates of changes. The 2011 emissions and subsequently contributions from these 2 sectors are underestimated.

3.4.1. Source attribution changes of air pollution—attributable premature deaths

Anthropogenic emission reductions between 2011 and 2016 resulted in net decreases of 76 (28–149) premature deaths (–29%) in DC. For PM_{2.5}-attributable premature deaths, decreases of 59%, 35%, 34%, and 30% in the EGU, other-point, nonroad, and residential sectors, respectively, were the largest changes. Although on-road vehicle absolute contributions to premature deaths decreased more (12; 4–23), than both the nonroad (10; 4–19), and residential (5; 2–10) sectors, due to its large contribution in 2011, the on-road vehicle contributions had a smaller percentage difference at 24%.

 O_3 -attributable premature deaths decreased overall between 2011 and 2016. Five of the 6 considered sectors had O_3 -attributable health impact reductions between 2011 and 2016: other-point (50%), EGU (28%), on-road (27%), nonroad (21%), and residential (11%). Meanwhile, one sector had increased O_3 -attributable premature deaths: shipping (86%). This breakdown is similar to that of $PM_{2.5}$ where emission reductions from all but one (shipping) of the 7 considered sectors led to reductions in $PM_{2.5}$ -related premature deaths; note that there is one fewer sector (agriculture) in this comparison for O_3 owing to its negligible VOC emissions.

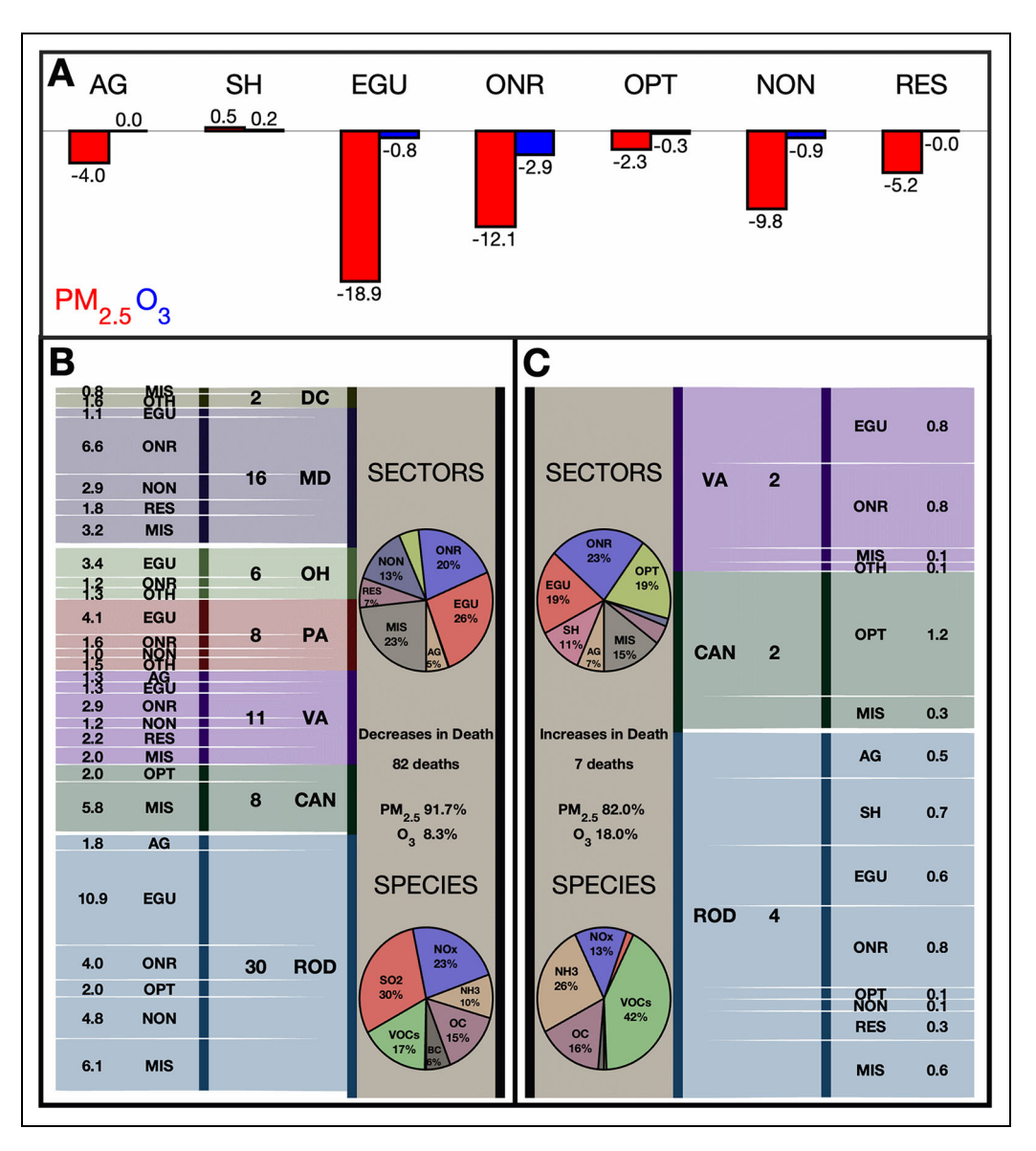


Figure 9. Changes in the sources of pollution-related premature deaths between 2011 and 2016. Source attribution of changes in pollution-related premature death between 2011 and 2016 considering (A) net changes in PM_{2.5} and O₃ exposure contributions, broken down further by (B) decreases and (C) increases of air pollution–related premature deaths. Pie charts indicate domain-wide proportions of sectors and species that contribute to decreases and increases; categories that contributed less than 5% are not labeled. Additionally, state contributions, and their sectoral contributions, to decreases and increases are included in the columns. DOI: https://doi.org/10.1525/elementa.2021.00043.f9

Overall, EGU emission reductions were proportionally much more impactful for PM_{2.5} than for O₃, while on-road emission reductions were proportionally more impactful for O₃ than for PM_{2.5}. For EGU reductions, it is possible that the severity of the difference between PM_{2.5} and O₃ impacts is reduced when considering the unaccounted for "surface" component of EGU emissions; however, since this surface level EGU component is a small fraction at the national level, it likely has only a minor impact.

We next consider the source attribution of these exposure contributions broken down by death decreases (**Figure 9B**) as distinct from increases (**Figure 9C**) to capture the different source groups responsible for changes in health impacts. We define "decreases" to be any species,

sector, and region combination that had a decreased relative contribution between 2011 and 2016 while "increases" are defined as any species, sector, and region combinations that had an increased relative contribution between 2011 and 2016. Although we avoid comparing the surface, oil and gas, and industry sector contribution changes directly as mentioned above, we do consider overall changes from these sectors in a "miscellaneous" group. Total decreases were over 11 times larger than increases, which should be kept in mind when comparing these 2 groups directly.

The sectors whose emissions contributed to largest relative decreases in air pollution—attributable premature deaths between 2011 and 2016 were the EGU (56%),

other-point (36%), nonroad (32%), residential (30%), and on-road (25%). Of the 20 (10-34) fewer deaths contributed by the EGU sector, a majority came from emissions in 4 regions: Pennsylvania (20%), Ohio (17%), West Virginia (11%), and Kentucky (6%). Net EGU emission contributions from Virginia were relatively unchanged as the increases and decreases were of relatively similar magnitude; however, this could be in part attributable to our underestimate of EGU emissions in 2011 from not accounting for nonplume rise EGU emissions. Most of the decreased nonroad contributions came from 2 regions: Maryland (29%) and Virginia (12%). A majority of the 15 (4-30) fewer premature deaths contributed by the on-road sector came from Maryland (44%) and Virginia (13%). The sector with the largest relative increases to air pollution-attributable premature deaths was shipping, with a 77% increase.

Proportionally, contributions from OC were similar in both decreases and increases. SO2 reductions, however, were responsible for 29% of premature death reductions and less than 2% of premature death increases. This large, reduced contribution from SO₂ is attributable to the closing of EGUs, especially in states in the Ohio River Valley, along with SO₂ emission reductions in EGUs that remained open. Of all SO2 reductions, the EGU sector was responsible for 74% of decreases between 2011 and 2016. Regionally, the largest SO₂ reductions came from Ohio (15%), Pennsylvania (14%), and West Virginia (9%). Overall VOC contributions decreased by 12 (4–26) premature deaths; however, contributions from VOCs proportionally were larger in increases (43%) than decreases (17%). Regionally, all states in the eastern United States had net decreases in pollution-related premature death contributions between 2011 and 2016. Maryland was responsible for 19% of air pollution-attributable premature death decreases while contributing very little to increases.

3.4.2. Source attribution changes of NO₂-attributable pediatric asthma cases

Between 2011 and 2016, anthropogenic emission reductions resulted in a net decrease of 227 (2-617) new pediatric asthma cases. In **Figure 10A**, we consider these net decreases across all sectors. Overall, the on-road, nonroad, and EGU sectors were responsible for the most reductions in asthma cases, despite increased contributions from shipping. Decreases in on-road vehicle emissions had larger health benefits for pediatric asthma cases (-56%) than for premature deaths (-24%). Again, we consider decreases (Figure 10B) as distinct from increases (Figure **10C**). The on-road (63%) and nonroad (12%) sectors made up large fractions of decreases and contributed very little to increases. The shipping sector (13%) made up large fractions of increases and contributed very little to decreases. The only sector that contributed both large increases and decreases was the EGU sector; however, large increases could in part be explained by our not accounting for nonplume rise EGU emissions in the 2011 sectoral definition.

The large contributions to both decrease and increases in the EGU sector can be further evaluated by considering

the spatial distribution of contributions. In Virginia, there was a net increase in new pediatric asthma case contributions from EGUs between 2011 and 2016. Despite reductions from the on-road and nonroad sectors, increased contributions partially from EGUs led to an overall increased contribution from Virginia. It is possible that this increased contribution from EGUs in Virginia is partially attributable to our underestimating of EGU emissions in 2011; however, based on the national breakdown of plume-rise and surface EGU emissions, this is unlikely a large enough factor to entirely account for positive contributions. In all other states, however, EGU contributions decreased; this is why overall there were both relatively large increases and decreases in new pediatric asthma case contributions from the EGU sector. Every state besides Virginia contributed less asthma cases to DC in 2011 than in 2016. Emission changes in Maryland alone majorly benefited DC by contributing 170 (30–368) fewer asthma cases, which made up 75% of all decreased reductions. Emission decreases from DC, Pennsylvania, and Ohio resulted in reduced pediatric asthma incidence contributions with net decreases of 16 (1–39), 13 (0–35), and 7 (1– 15), respectively. Across all states with major decreases, the on-road sector was always the sector with the greatest decrease in contributions to NO₂-attributable new pediatric asthma cases.

3.4.3. Source attribution changes from all health impacts

Considering both premature deaths and pediatric asthma cases, reductions in the health burden of DC between 2011 and 2016 were primarily due to decreased on-road, EGU, and nonroad contributions despite increased contributions from shipping. Of the large regional health impact contributors, emission decreases in Maryland were the most beneficial to DC followed by DC itself and Pennsylvania. The health impacts associated with changes in emissions in Virginia were more mixed; emissions from Virginia contributed less to premature deaths but more to asthma cases in this 5-year time frame. Since we use the same sensitivities for both 2011 and 2016, the above difference is directly comparing the changes attributable to emission changes and not from changes in meteorology. Across both health impacts, we estimate net decreases in EGU contributions of at least 20 (10–34), fewer premature deaths, and 26 (2-65) fewer new asthma cases.

3.5. Uncertainty analysis

Uncertainty is inherent in the 3 main steps of our analysis: the forward model calculation of pollutant exposures, the adjoint model calculation of pollutant exposure sensitivities, and the health impact analysis. While uncertainty in the first 2 steps is addressed in the following paragraphs and accounted for through the inclusion of satellite-derived data, it is not formally considered in the uncertainty bounds we report for the health impacts; for the latter, we only consider the uncertainty in the health impact calculation as it is typically (Lee et al., 2015; Anenberg et al., 2019b) the highest source of uncertainty in health impact assessments (which we find to also be the

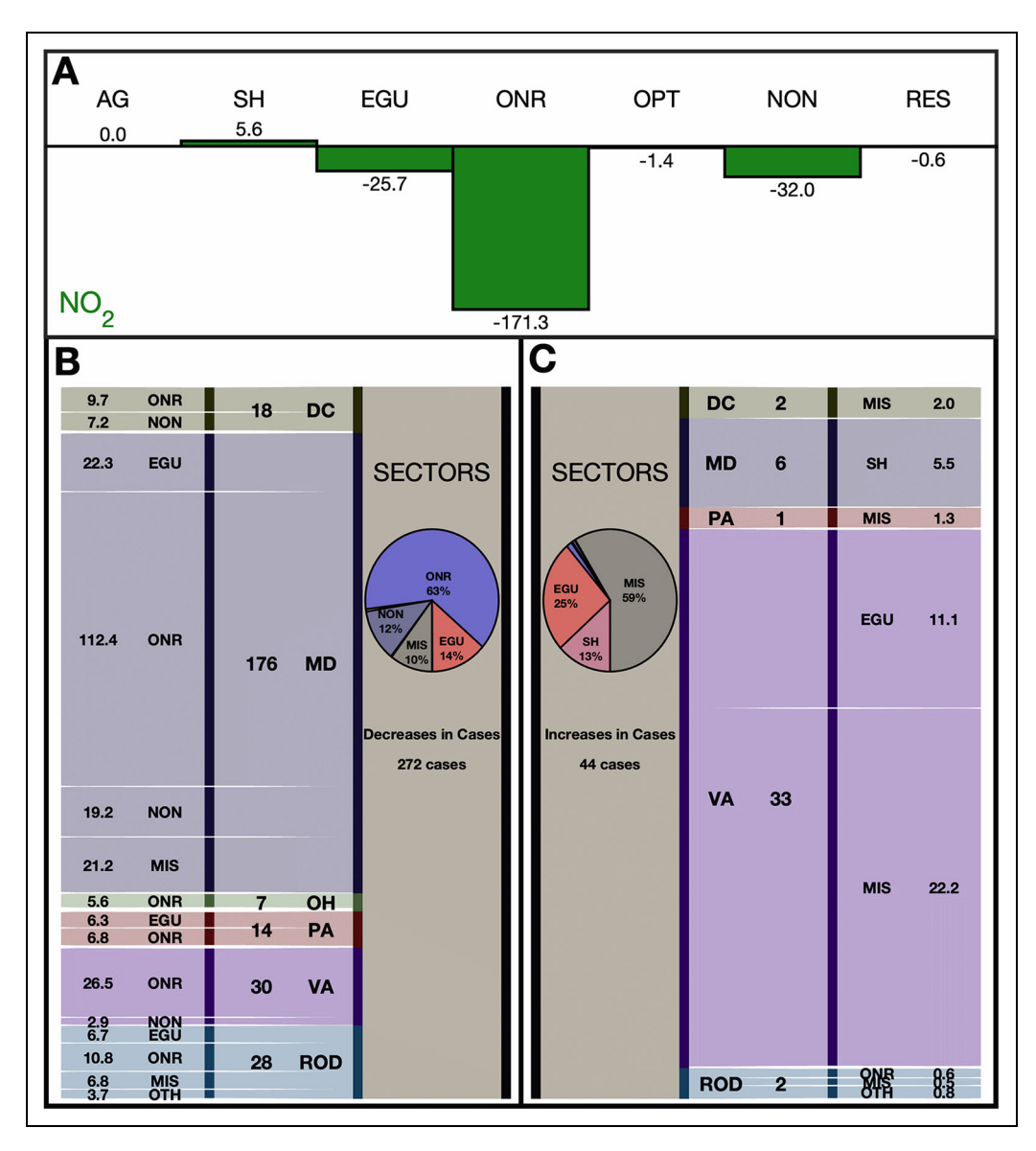


Figure 10. Changes in pollution-related new asthma cases between 2011 and 2016. Source attribution of changes in pollution-related new asthma cases between 2011 and 2016 considering (A) net changes in NO₂ exposure contributions, broken down further by (B) death decreases and (C) increases of air pollution—related new pediatric asthma cases. Pie charts indicate domain-wide proportions of sectors and species that contribute to decreases and increases; categories that contributed less than 5% are not labeled. Additionally, state contributions, and their sectoral contributions, to decreases and increases are included in the columns. DOI: https://doi.org/10.1525/elementa.2021.00043.f10

case here as explained below) and because of the difficulty in specifying the covariance between the health impact calculation and the other sources of uncertainty that would be needed to rigorously combine them.

Uncertainty in forward model calculations of pollutant concentrations is introduced by meteorological and emissions inputs and approximations or omissions in the processes or chemistry represented by the model. To compensate for forward model biases, for PM_{2.5}, we perform a satellite rescaling to replace the simulated concentrations with a satellite-derived product that performs well against out of sample cross-validated in situ observations ($R^2 = 0.81$; van Donkelaar et al., 2016). By incorporating satellite-derived data, there is a reduction in bias from

+28% to +22% for PM_{2.5}. Additionally, we apply a satellite downscaling to the simulated NO₂ columns; here, we perform a downscaling, as opposed to a rescaling, because the simulation year, 2011, differs from the satellite product years, 2018–2019. Uncertainty in the O₃ simulation is the greatest since it is the only pollutant we consider without a satellite-based correction. A positive O₃ bias has been identified previously in GEOS-Chem (Travis et al., 2016) and in other models (Butler et al., 2020; Turnock et al., 2020) and arises in part due to comparing O₃ mole fractions from the lowest model level (approximately 65 m) to in situ observations much closer to the ground (approximately 2 m). By adjusting lowest model level maximum 8-h daily average (MDA8) O₃ (midpoint at 65 m) to

the height of aircraft observations (10 m), one study (Travis and Jacob, 2019) estimated an improvement in bias from +8 ppb to +5 ppb in the southeast United States in August-September 2013 compared to observations from an aircraft campaign. Based on a simple global simulation conducted by us at the $2^{\circ} \times 2.5^{\circ}$ for 2010, we estimate that over the 6-month peak period in the grid cell containing DC correcting to the 2 m height would lead to a reduction in NMB of 10% for MDA1 O₃ with daily varying reductions ranging from 2% to 30%. Generally, errors in model concentrations reflect the uncertainty introduced from model inputs like meteorological fields and emissions; artifacts in the output of our simulations formed from uncertainties in the input are thus partially captured when comparing concentrations and exposures to in situ observations for 2011. When considering the results for 2016, there would be artifacts from the 2011 simulation that would differ if we instead considered inputs for 2016; we do not consider this uncertainty in our analysis. Overall, we calculate mean concentrations, in the form of the exposure metrics, that are 122%, 125%, and 112% the values of the comparable in situ observations for PM_{2.5}, O₃, and NO₂. All of these biases are positive, so we likely overestimate source contributions slightly; however, these errors are much smaller than those introduced in other steps.

The adjoint calculation uncertainty comes from this method providing only a first-order linear approximation of source contributions. For OC and BC, there are no errors owing to nonlinear effects as the model representation of these species is linear. For NH₃, NO_x, SO₂, and VOCs, since this first-order approximation neglects higher order sensitivities, the sensitivities calculated here will not necessarily represent the changes in pollutant exposures for large emissions perturbations. When comparing 2011 and 2016 directly, the overall emission perturbations are likely smaller than the range in which this approximation breaks down; however, this is not necessarily true when considering the 100% perturbations in individual years. We conservatively consider uncertainty introduced through this nonlinearity by treating the sum of total contributions as the central value and calculate a lower and upper bound informed by the difference between the cost functions and the sum of total contributions. While we consider uncertainty bounds for all 3 pollutants, we apply a correction factor specifically for O₃, the most nonlinear of these pollutants for the conditions of this study, by scaling adjoint sensitivities to the cost function values; a similar approach has been done in another study (Ni et al., 2018). Considering all of this, the anthropogenic contributions are 16 (12–20) ug/m³, 75 (33–116) ppbv, and 19 (16–22) ppbv for PM_{2.5}, O₃, and NO₂, respectively. Comparing these ranges to the central estimate as a percentage difference, we estimate errors of 24%, 55%, and 18% for the same pollutants, respectively. Our estimates of the changes in source contributions between 2011 and 2016 are likely more robust than the absolute contribution estimates for either of these years; these uncertainties are, however, smaller than those in the health impact assessment. We also note the source attributions are more accurate in a relative sense than an absolute sense. Overall, we

choose not to combine these uncertainties with those from the health impact calculation as we lack information on the covariance between these 2 quantities; however, both sources of uncertainty are important to consider.

Previous studies have considered to what extent the linear (first order) response is accurate.

For O₃, the root mean square error in first-order contributions ranged from 1 to 4 ppb and 0.5 to 2.5 ppb higher than higher order contributions for NO_x and VOC perturbations, respectively (Hakami et al., 2004), for 50% perturbations. For PM_{2.5}, second-order sensitivities were calculated by Koo (2011) by performing separate adjoint calculations with aviation emissions turned off at the global $2^{\circ} \times 2.5^{\circ}$ resolution in GEOS-Chem. Using these sensitivities, first-order uncertainty ranged in magnitude as (all in units of $10^{-9} \left(\frac{\text{ug}}{\text{m}^3}\right) / \left(\frac{\text{kg}}{\text{m}^2 \text{s}}\right)$): for NH₃, -3 to 3; for NO_x, -2 to 2; and for SO₂, -0.4 to 0.4. For comparison, the firstorder sensitivities of these precursors ranged in magnitude as (all in units of $10^{-9} \left(\frac{\text{ug}}{\text{m}^3}\right) / \left(\frac{\text{kg}}{\text{m}^2\text{s}}\right)$): for NH₃, -150 to 150; for NO_x, -60 to 60; and for SO₂, -60 to 60. Uncertainty in the forward and adjoint modeling will have the greatest impact on the overall magnitude of contributions, as opposed to their relative contributions. Because of this, relative results in our study are more accurate than overall totals.

The health impact analysis includes uncertainty in the population estimates, the health outcome mortalities and incidence, and the exposure response relationships used to estimate the health impacts. The former is quantified using the lower and upper bounds of the population, mortality, incidence, and risk data reported by the GBD 2019. Epidemiological studies include uncertainty bounds in the exposure response relationships. By considering the lower and upper bounds across all 3 of these factors, we can quantify uncertainty bounds around the total pollution-relation health impacts can be calculated. There is also additional uncertainty in the health impact analysis introduced by the choice of the concentration-response relationship used to estimate premature deaths. To account for this for PM_{2.5}, we reran our calculations using the GEMM (Burnett et al., 2018) model and compared them to the GBD 2019 estimates. For just PM_{2.5}, the GEMM estimated premature deaths of 319 in 2011 and 223 in 2016; this is larger than the GBD 2019 estimates of 237 in 2011 and 167 in 2016.

Overall, we find that for each unique contribution ($\geq 1 \times 10^{-9}$) to health impacts in DC, impacts range (as a percentage difference comparing the central estimate to both of the bounds) from -46% to +61%, -94% to +145%, and -65% to +60% for PM_{2.5}, O₃, and NO₂, respectively.

Across all 3 pollutants, both the lower and upper bounds of uncertainty in the health impact calculation were larger than that introduced from the local-linear adjoint approximation, the other large source of uncertainty in this study.

4. Conclusion

In this study, we characterized the sources of air pollution—related health impacts in DC in 2011 and quantified

changes in these health impacts between 2011 and 2016. Anthropogenic emissions contributed an estimated 263 (130–444) PM_{2.5}- and O₃-attributable premature deaths and 1,120 (391–1,795) NO₂-attributable pediatric asthma cases in Washington, DC, in 2011. PM_{2.5} exposure had the most diverse sectoral sources of all 3 pollutants due in large part to the differing sources of its precursor species.

Between 2011 and 2016, decreases in pollution-related health impacts occurred due to decreases in anthropogenic emissions. Anthropogenic emission reductions resulted in an estimated 76 (28–149) fewer air pollution– related premature deaths and 227 (2-617) fewer NO₂attributable pediatric asthma cases in DC between these years. Decreases in air pollution-attributable premature deaths primarily came from improvements in the EGU. on-road, and nonroad sectors. These decreases present evidence of the health benefits of closing coal power plants near DC and transitioning to cleaner fuels for energy generation. The agriculture sector showed little change in contributions between 2011 and 2016. Decreased contributions to NO₂-attributable pediatric asthma cases came primarily from the on-road sector (63%) although decreases from the nonroad and EGU sectors also occurred. From Virginia, EGU contributions to NO₂-attributable new asthma cases likely increased between 2011 and 2016; at most, EGUs made up 34% of all increases in Virginia. Reduction in emissions from Maryland were the most responsible for decreases in asthma incidence (74%).

The novel approach presented in this work is applicable to any region that falls within a nested domain at $0.5^{\circ} \times 0.667^{\circ}$ or finer spatial resolution in GEOS-Chem and for which a local or regional sector and species-specific emissions inventory is available. By incorporating satellite-derived surface-level pollutant concentrations into our analysis, pollutant concentrations better match in situ data and allow for more accurate calculation of exposures and health impacts. By calculating adjoint sensitivities at a daily time step, contributions from individual days can be derived allowing for the identification of unique emission periods or events. By aggregating daily contributions to the monthly timescale, seasonality of contributions to pollutants can be identified.

There are multiple sources of uncertainty that should be considered when interpreting these results. The accuracy of our simulated pollutants, compared to observations, depends upon the accuracy of the emissions inventories and meteorological fields that are input into our simulations; since we are presenting results at fine temporal resolution, and since uncertainties in these 2 inputs are likely larger at finer temporal resolutions, any uncertainty at the daily timescale would be higher than for monthly or annual results. Our modeling setup does not consider fugitive dust which could underestimate total PM_{2.5} and in turn the relative sectoral contributions, although dust is typically low in the eastern United States. The adjoint sensitivities are calculated at a coarse spatial resolution of $0.5^{\circ} \times 0.667^{\circ}$; at this resolution, it is impossible to resolve fine scale sensitivities which results in an underestimate of contributions near DC. As the coarse scales of the sensitivity calculations performed here may

underestimate this hyperlocal (within the district) sensitivity, we avoid commenting on the distribution of contributions within versus outside of the district and primarily focus our analysis on the distribution and characterization of sources outside of this area.

Additionally, the response sensitivity relationship used in the contribution calculation is only a first-order approximation that is the most valid close to the input emission magnitudes. When we consider larger changes in emissions, as we do in our analysis for annual source contributions, the nonlinear emission responses are larger, and thus, our results are less accurate. When calculating contributions for 2016, we combine 2016 emissions with sensitivities calculated with respect to 2011 pollutant exposures; this could introduce error due to year-to-year changes in meteorology and evolution of the chemical regime between these 2 periods. To mitigate the uncertainty introduced by this, we only consider annual results for analysis of the difference between 2016 and 2011 and ignore smaller timescales (e.g., daily contributions). When incorporating NO₂ satellite data into this analysis, we use TROPOMI columns oversampled for a period including parts of 2018 and 2019 since this is the earliest that TRO-POMI data are available. This downscaling relationship applied to the simulation for 2011 incorporates subgrid variability from TROPOMI columns in 2018 and 2019 which are not necessarily consistent with subgrid variabilities for 2011. While OMI columns are available for the year of our simulation, the improved spatial resolution of the TROPOMI product was more beneficial for resolving urban-scale pollutant mole fractions. Beyond all these uncertainties, there are large inherent uncertainties in the risk exposure relationships used to estimate health impacts (Anenberg et al., 2010; Cohen et al., 2017; Anenberg et al., 2018; Achakulwisut et al., 2019).

With these uncertainties in mind, the results of this work have a range of air quality policy implications. While the air quality policy focus in DC has primarily been on O₃ due to its current nonattainment of the 2015 8-h max O₃ NAAQS, it was reductions in PM_{2.5} not O₃ that accrued more health benefits between 2011 and 2016. By considering the cobenefits from emission reductions of reduced PM_{2.5}-attibutable premature deaths and NO₂-attributable pediatric asthma cases, the health benefits of these reductions are made clear even if the NAAQS attainment status of O₃ remains unchanged. Such cobenefits allow local governments to inform their citizens of the effectiveness of emission reduction policies and actions. Calculating contributions at a fine temporal resolution makes it possible to identify the impacts that emissions from an individual day have on pollutant exposures and their associated health impacts. The approach outlined in this work presents a framework for characterizing the sources of pollution at the urban scale that is applicable to other cities throughout the world. However, calculating sensitivities at the coarse $0.5^{\circ} \times 0.667^{\circ}$ resolution presents a challenge for accurately identifying the impacts that city emissions have on the city itself. Using finer spatial resolution emissions can partially mitigate this problem; however, ultimately this is a limitation of this framework and

presents a need for further development of urban-scale sensitivity calculations. Despite this limitation, our results still show the value for multijurisdictional cooperation in air quality management across municipal, county, state, and federal levels.

Data accessibility statement

The following data sets were generated:

- Nawaz et al. (2021; daily adjoint sensitivities of PM2.5, O3, and NO2), CU Scholar Database, https://scholar.colorado.edu/concern/datasets/ s7526d65d.
- Nawaz et al. (2021; GEOS-Chem simulated pollutant concentrations), CU Scholar Database, https://scholar.colorado.edu/concern/datasets/s7526d65d.
- Contribution calculation scripts: CU Scholar Database, https://scholar.colorado.edu/concern/ datasets/s7526d65d.

Supplemental files

The supplemental files for this article can be found as follows:

Figures S1-S16. Table S1. PDF

Funding

This project was funded by NASA grants NNX16AQ26G and 80NSSC19K0193 and NSF grant AGS-1822664.

Competing interests

There are no competing interests to disclose.

Author contributions

Contributed to conception and design: MON, DKH, SCA, DWG.

Contributed to acquisition of data: MON, CH.

Contributed to analysis and interpretation of data: MON, DKH, SCA, DWG, JLJ, BN, HC, ZQ, CH.

Drafted and/or revised this article: MON, DKH, SCA, DWG, BN, HC, ZQ, CH.

Approved the submitted version for publication: MON, DKH, SCA, DWG, JLJ, BN, HC, ZQ, CH.

References

- Achakulwisut, P, Brauer, M, Hystad, P, Anenberg, SC. 2019. Global, national, and urban burdens of paediatric asthma incidence attributable to ambient NO2 pollution: Estimates from global datasets. *The Lancet Planetary Health* **3**: e166–e178. DOI: http://dx.doi.org/10.1016/S2542-5196(19)30046-4.
- Anenberg, SC, Achakulwisut, P, Brauer, M, Moran, D, Apte, JS, Henze, DK. 2019a. Particulate matterattributable mortality and relationships with carbon dioxide in 250 urban areas worldwide. *Scientific Reports* 9: 11552. DOI: http://dx.doi.org/10.1038/s41598-019-48057-9.
- Anenberg, SC, Henze, DK, Tinney, V, Kinney, PL, Raich, W, Fann, N, Malley, CS, Roman, H, Lamsal, L,

- Duncan, B, Martin, RV, van Donkelaar, A, Brauer, M, Doherty, R, Jonson, JE, Davila, Y, Sudo, K, Kuylenstierna, JCI. 2018. Estimates of the global burden of ambient PM2.5, ozone, and NO2 on asthma incidence and emergency room visits. *Environmental Health Perspectives* **126**: 107004. DOI: http://dx.doi.org/10.1289/EHP3766.
- Anenberg, SC, Horowitz, LW, Tong, DQ, West, JJ. 2010. An estimate of the global burden of anthropogenic ozone and fine particulate matter on premature human mortality using atmospheric modeling. *Environmental Health Perspectives* **118**: 1189–1195. DOI: http://dx.doi.org/10.1289/ehp.0901220.
- Anenberg, SC, Miller, J, Henze, DK, Minjares, R, Achakulwisut, P. 2019b. The global burden of transportation tailpipe emissions on air pollution-related mortality in 2010 and 2015. *Environmental Research Letters* 14: 094012. DOI: http://dx.doi.org/10. 1088/1748-9326/ab35fc.
- Burnett, R, Chen, H, Szyszkowicz, M, Fann, N, Hubbell, B, Pope, CA 3rd, Apte, JS, Brauer, M, Cohen, A, Weichenthal, S, Coggins, J, Di, Q, Brunekreef, B, Frostad, J, Lim, SS, Kan, H, Walker, KD, Thurston, GD, Hayes, RB, Lim, CC, Turner, MC, Jerrett, M, Krewski, D, Gapstur, SM, Diver, WR, Ostro, B, Goldberg, D, Crouse, DL, Martin, RV, Peters, P, Pinault, L, Tjepkema, M, van Donkelaar, A, Villeneuve, PJ, Miller, AB, Yin, P, Zhou, M, Wang, L, Janssen, NAH, Marra, M, Atkinson, RW, Tsang, H, Quoc Thach, T, Cannon, JB, Allen, RT, Hart, JE, Laden, F, Cesaroni, G, Forastiere, F, Weinmayr, G, Jaensch, A, Nagel, G, Concin, H, Spadaro, JV. 2018. Global estimates of mortality associated with long-term exposure to outdoor fine particulate matter. Proceedings of the National Academy Science **115**: 9592–9597. DOI: http://dx.doi.org/10.1073/ pnas.1803222115.
- Burnett, RT, Pope, CA 3rd, Ezzati, M, Olives, C, Lim, SS, Mehta, S, Shin, HH, Singh, G, Hubbell, B, Brauer, M, Anderson, HR, Smith, KR, Balmes, JR, Bruce, NG, Kan, H, Laden, F, Prüss-Ustün, A, Turner, MC, Gapstur, SM, Diver, WR, Cohen, A. 2014. An integrated risk function for estimating the global burden of disease attributable to ambient fine particulate matter exposure. *Environmental Health Perspectives* 122: 397–403. DOI: http://dx.doi.org/10.1289/ehp.1307049.
- **Butler, T, Lupascu, A, Nalam, A.** 2020. Attribution of ground-level ozone to anthropogenic and natural sources of nitrogen oxides and reactive carbon in a global chemical transport model. *Atmospheric Chemistry and Physics* **20**: 10707–10731. DOI: http://dx.doi.org/10.5194/acp-20-10707-2020.
- Canty, TP, Hembeck, L, Vinciguerra, TP, Anderson, DC, Goldberg, DL, Carpenter, SF, Allen, DJ, Loughner, CP, Salawitch, RJ, Dickerson, RR. 2015. Ozone and NO_x chemistry in the eastern US: evaluation of CMAQ/CB05 with satellite (OMI) data. *Atmospheric Chemistry and Physics* **15**: 10965–10982. DOI: http://dx.doi.org/10.5194/acp-15-10965-2015.

- Center for International Earth Science Information Network. 2018. Gridded population of the world. Version 4 (GPWv4) [WWW Document]. Available at http://dx.doi.org/10.7927/H4JW8BX5. Accessed 6 December 2020.
- Cohen, AJ, Brauer, M, Burnett, R, Anderson, HR, Frostad, J, Estep, K, Balakrishnan, K, Brunekreef, B, Dandona, L, Dandona, R, Feigin, V, Freedman, G, Hubbell, B, Jobling, A, Kan, H, Knibbs, L, Liu, Y, Martin, R, Morawska, L, Pope, CA 3rd, Shin, H, Straif, K, Shaddick, G, Thomas, M, van Dingenen, R, van Donkelaar, A, Vos, T, Murray, CJL, Forouzanfar, MH. 2017. Estimates and 25-year trends of the global burden of disease attributable to ambient air pollution: An analysis of data from the Global Burden of Diseases Study 2015. *The Lancet* 389: 1907–1918. DOI: http://dx.doi.org/10.1016/S0140-6736(17)30505-6.
- Cooper, MJ, Martin, RV, McLinden, CA, Brook, JR. 2020. Inferring ground-level nitrogen dioxide concentrations at fine spatial resolution applied to the TROPOMI satellite instrument. *Environmental Research Letters* **15**: 104013. DOI: http://dx.doi.org/10.1088/1748-9326/aba3a5.
- Davidson, K, Fann, N, Zawacki, M, Fulcher, C, Baker, KR. 2020. The recent and future health burden of the U.S. mobile sector apportioned by source. *Environmental Research Letters* **15**: 075009. DOI: http://dx.doi.org/10.1088/1748-9326/ab83a8.
- **DC** Department of Energy and Environment. 2019. Ambient air quality trends report (Trends Report), Ambient Air Quality Trends Report. Washington DC: DC Department of Energy and Environment.
- DC Office of Planning, DC Department of Energy and Environment. 2018. Sustainable DC 2.0 plan. District of Columbia Office of Planning and District of Columbia Department of Energy and Environment.
- **Dedoussi, IC, Eastham, SD, Monier, E, Barrett, SRH.** 2020. Premature mortality related to United States cross-state air pollution. *Nature* **578**: 261–265. DOI: http://dx.doi.org/10.1038/s41586-020-1983-8.
- Doherty, RM, Heal, MR, O'Connor, FM. 2017. Climate change impacts on human health over Europe through its effect on air quality. *Environmental Health* 16: 118. DOI: http://dx.doi.org/10.1186/s12940-017-0325-2.
- **Environmental Protection Agency**. 2015. *NEI 2011 Technical support document*. Triangle Park, NC: U.S. Environmental Protection Agency Office of Air Quality Planning and Standard, Research.
- Goldberg, DL, Vinciguerra, TP, Anderson, DC, Hembeck, L, Canty, TP, Ehrman, SH, Martins, DK, Stauffer, RM, Thompson, AM, Salawitch, RJ, Dickerson, RR. 2016. CAMx ozone source attribution in the eastern United States using guidance from observations during DISCOVER-AQ Maryland. *Geophysical Research Letters* **43**: 2249–2258. DOI: http://dx.doi.org/10.1002/2015GL067332.
- Goodkind, AL, Tessum, CW, Coggins, JS, Hill, JD, Marshall, JD. 2019. Fine-scale damage estimates of

- particulate matter air pollution reveal opportunities for location-specific mitigation of emissions. *Proceedings of the National Academy of Sciences* **116**: 8775–8780. DOI: http://dx.doi.org/10.1073/pnas. 1816102116.
- **Guenther, A, Karl, T, Harley, P, Wiedinmyer, C, Palmer, PI, Geron, C**. 2006. Estimates of global terrestrial isoprene emissions using MEGAN (Model of Emissions of Gases and Aerosols from Nature). *Atmospheric Chemistry and Physics* **6**: 3181–3210. DOI: http://dx.doi.org/10.5194/acp-6-3181-2006.
- Guo, R, Deser, C, Terray, L, Lehner, F. 2019. Human influence on winter precipitation trends (1921– 2015) over North America and Eurasia revealed by dynamical adjustment. *Geophysical Research Letters* 46: 3426–3434. DOI: http://dx.doi.org/10.1029/ 2018GL081316.
- Hakami, A, Odman, MT, Russell, AG. 2004. Nonlinearity in atmospheric response: A direct sensitivity analysis approach. *Journal of Geophysical Research Atmospheres* **109**. DOI: http://dx.doi.org/10.1029/2003JD004502.
- Hammer, MS, van Donkelaar, A, Li, C, Lyapustin, A, Sayer, AM, Hsu, NC, Levy, RC, Garay, MJ, Kalashnikova, OV, Kahn, RA, Brauer, M, Apte, JS, Henze, DK, Zhang, L, Zhang, Q, Ford, B, Pierce, JR, Martin, RV. 2020. Global estimates and long-term trends of fine particulate matter concentrations (1998–2018). *Environmental Science & Technology* **54**: 7879–7890. DOI: http://dx.doi.org/10.1021/acs.est.0c01764.
- He, H, Loughner, CP, Stehr, JW, Arkinson, HL, Brent, LC, Follette-Cook, MB, Tzortziou, MA, Pickering, KE, Thompson, AM, Martins, DK, Diskin, GS, Anderson, BE, Crawford, JH, Weinheimer, AJ, Lee, P, Hains, JC, Dickerson, RR. 2014. An elevated reservoir of air pollutants over the Mid-Atlantic States during the 2011 DISCOVER-AQ campaign: Airborne measurements and numerical simulations. *Atmospheric Environment* 85: 18–30. DOI: http://dx.doi.org/10.1016/j.atmosenv.2013.11.039.
- Henze, DK, Hakami, A, Seinfeld, JH. 2007. Development of the adjoint of GEOS-Chem. *Atmospheric Chemistry and Physics* **7**: 2413–2433. DOI: http://dx.doi.org/10.5194/acp-7-2413-2007.
- Jerrett, M, Burnett, RT, Pope, CA, Ito, K, Thurston, G, Krewski, D, Shi, Y, Calle, E, Thun, M. 2009. Long-term ozone exposure and mortality. *The New England Journal of Medicine* **360**: 1085–1095. DOI: http://dx.doi.org/10.1056/NEJMoa0803894.
- Jimenez, JL, Canagaratna, MR, Donahue, NM, Prevot, AS, Zhang, Q, Kroll, JH, DeCarlo, PF, Allan, JD, Coe, H, Ng, NL, Aiken, AC, Docherty, KS, Ulbrich, IM, Grieshop, AP, Robinson, AL, Duplissy, J, Smith, JD, Wilson, KR, Lanz, VA, Hueglin, C, Sun, YL, Tian, J, Laaksonen, A, Raatikainen, T, Rautiainen, J, Vaattovaara, P, Ehn, M, Kulmala, M, Tomlinson, JM, Collins, DR, Cubison, MJ, Dunlea, EJ, Huffman, JA, Onasch, TB, Alfarra, MR, Williams, PI, Bower, K, Kondo, Y, Schneider, J,

- Drewnick, F, Borrmann, S, Weimer, S, Demerjian, K, Salcedo, D, Cottrell, L, Griffin, R, Takami, A, Miyoshi, T, Hatakeyama, S, Shimono, A, Sun, JY, Zhang, YM, Dzepina, K, Kimmel, JR, Sueper, D, Jayne, JT, Herndon, SC, Trimborn, AM, Williams, LR, Wood, EC, Middlebrook, AM, Kolb, CE, Baltensperger, U, Worsnop, DR. 2009. Evolution of organic aerosols in the atmosphere. *Science* **326**: 1525–1529. DOI: http://dx.doi.org/10.1126/science.1180353.
- Jolley, GJ, Khalaf, C, Michaud, G, Sandler, AM. 2019. The economic, fiscal, and workforce impacts of coalfired power plant closures in Appalachian Ohio. *Regional Science Policy & Practice* **11**: 403–422. DOI: http://dx.doi.org/10.1111/rsp3.12191.
- Kim ,PS, Jacob, DJ, Fisher, JA, Travis, K, Yu, K, Zhu, L, Yantosca, RM, Sulprizio, MP, Jimenez, JL, Campuzano-Jost, P, Froyd, KD, Liao, J, Hair, JW, Fenn, MA, Butler, CF, Wagner, NL, Gordon, TD, Welti, A, Wennberg, PO, Crounse, JD, St. Clair JM, Teng, AP, Millet, DB, Schwarz, JP, Markovic, MZ, Perring, AE. 2015. Sources, seasonality, and trends of southeast US aerosol: An integrated analysis of surface, aircraft, and satellite observations with the GEOS-Chem chemical transport model. *Atmospheric Chemistry and Physics* 15: 10411–10433. DOI: http://dx.doi.org/10.5194/acp-15-10411-2015.
- **Koo, J.** 2011. Adjoint sensitivity analysis of the intercontinental impacts of aviation emissions on air quality and health [M.S. thesis]. Cambridge, MA: Massachusetts Institute of Technology School of Engineering.
- Kousky, V, Ropelewski, C. 1997. Northern hemisphere seasonal variations [WWW Document]. Tropospheric Seas. Varying Mean Clim. West. Hemisphere. Available at https://www.cpc.ncep.noaa.gov/products/precip/atlas3/cont_chp4.html. Accessed 11 October 2020.
- Lacey, FG, Henze, DK, Lee, CJ, van Donkelaar, A, Martin, RV. 2017. Transient climate and ambient health impacts due to national solid fuel cookstove emissions. *Proceedings of the National Academy of Science* 114: 1269–1274. DOI: http://dx.doi.org/10.1073/pnas.1612430114.
- Lee, CJ, Martin, RV, Henze, DK, Brauer, M, Cohen, A, van Donkelaar, A. 2015. Response of global particulate-matter-related mortality to changes in local precursor emissions. *Environmental Science & Technology* **49**: 4335–4344. DOI: http://dx.doi.org/10.1021/acs.est.5b00873.
- Loughner, CP, Follette-Cook, MB, Duncan, BN, Hains, J, Pickering, KE, Moy, J, Tzortziou, M. 2020. The benefits of lower ozone due to air pollution emission reductions (2002–2011) in the Eastern United States during extreme heat. *Journal of the Air & Waste Management Association* 70: 193–205. DOI: http://dx.doi.org/10.1080/10962247.2019. 1694089.
- Loughner, CP, Tzortziou, M, Follette-Cook, M, Pickering, KE, Goldberg, D, Satam, C, Weinheimer, A,

- **Crawford, JH, Knapp, DJ, Montzka, DD, Diskin, GS, Dickerson, RR.** 2014. Impact of Bay-breeze circulations on surface air quality and boundary layer export. *Journal of Applied Meteorology and Climatology.* **53**: 1697–1713. DOI: http://dx.doi.org/10.1175/JAMC-D-13-0323.1.
- Malley, CS, Henze, DK, Kuylenstierna, JCI, Vallack, HW, Davila, Y, Anenberg, SC, Turner, MC, Ashmore, MR. 2017. Updated global estimates of respiratory mortality in adults ≥30 years of age attributable to long-term ozone exposure. *Environmental Health Perspectives* **125**: 087021. DOI: http://dx.doi.org/10.1289/EHP1390.
- McMurry, P, Shepherd, M, Vickery, J. eds. 2004. Particulate matter science for policy makers: A NARSTO assessment. Cambridge, UK: Cambridge University Press
- Moghani, M, Archer, CL, Mirzakhalili, A. 2018. The importance of transport to ozone pollution in the U.S. Mid-Atlantic. *Atmospheric Environment* **191**: 420–431. DOI: http://dx.doi.org/10.1016/j. atmosenv.2018.08.005.
- Murray, CJL, Aravkin, AY, Zheng, P, Abbafati, C, Abbas, KM, Abbasi-Kangevari, M, Abd-Allah, F, Abdelalim, A, Abdollahi, M, Abdollahpour, I, Abegaz, KH, Abolhassani, H, Aboyans, V, Abreu, LG, Abrigo, MRM, Abualhasan, A, Abu-Raddad, LJ, Abushouk, AI, Adabi, M, Adekanmbi, V, Adeoye, AM, Adetokunboh, OO, Adham, D, Advani, SM, Agarwal, G, Aghamir, SMK, Agrawal, A, Ahmad, T, Ahmadi, K, Ahmadi, M, Ahmadieh, H, Ahmed, MB, Akalu, TY, Akinyemi, RO, Akinyemiju, T, Akombi, B, Akunna, CJ, Alahdab, F, Al-Aly, Z, Alam, K, Alam, S, Alam, T, Alanezi, FM, Alanzi, TM, Alemu, B wassihun, Alhabib, KF, Ali, M, Ali, S, Alicandro, G, Alinia, C, Alipour, V, Alizade, H, Aljunid, SM, Alla, F, Allebeck, P, Almasi-Hashiani, A, Al-Mekhlafi, HM, Alonso, J, Altirkawi, KA, Amini-Rarani, M, Amiri, F, Amugsi, DA, Ancuceanu, R, Anderlini, D, Anderson, JA, Andrei, CL, Andrei, T, Angus, C, Anjomshoa, M, Ansari, F, Ansari-Moghaddam, A, Antonazzo, IC, Antonio, CAT, Antony, CM, Antriyandarti, E, Anvari, D, Anwer, R, Appiah, SCY, Arabloo, J, Arab-Zozani, M, Ariani, F, Armoon, B, Ärnlöv, J, Arzani, A, Asadi-Aliabadi, M, Asadi-Pooya, AA, Ashbaugh, C, Assmus, M, Atafar, Z, Atnafu, DD, Atout, MMW, Ausloos, F, Ausloos, M, Ayala Quintanilla, BP, Ayano, G, Ayanore, MA, Azari, S, Azarian, G, Azene, ZN, Badawi, A, Badiye, AD, Bahrami, MA, Bakhshaei, MH, Bakhtiari, A, Bakkannavar, SM, Baldasseroni, A, Ball, K, Ballew, SH, Balzi, D, Banach, M, Banerjee, SK, Bante, AB, Baraki, AG, Barker-Collo, SL, Bärnighausen, TW, Barrero, LH, Barthelemy, CM, Barua, L, Basu, S, Baune, BT, Bayati, M, Becker, JS, Bedi, N, Beghi, E, Béjot, Y, Bell, ML, Bennitt, FB, Bensenor, IM, Berhe, K, Berman, AE, Bhagavathula, AS, Bhageerathy, R, Bhala, N, Bhandari, D, Bhattacharyya, K, Bhutta, ZA, Bijani, A, Bikbov, B, Bin

Sayeed, MS, Biondi, A, Birihane, BM, Bisignano, C, Biswas, RK, Bitew, H, Bohlouli, S, Bohluli, M, Boon-Dooley, AS, Borges, G, Borzì, AM, Borzouei, S, Bosetti, C, Boufous, S, Braithwaite, D, Breitborde, NJK, Breitner, S, Brenner, H, Briant, PS, Briko, AN, Briko, NI, Britton, GB, Bryazka, D, Bumgarner, BR, Burkart, K, Burnett, RT, Burugina Nagaraja, S, Butt, ZA, Caetano dos Santos, FL, Cahill, LE, Cámera, LLA, Campos-Nonato, IR, Cárdenas, R, Carreras, G, Carrero, JJ, Carvalho, F, Castaldelli-Maia, JM, Castañeda-Orjuela, CA, Castelpietra, G, Castro, F, Causey, K, Cederroth, CR, Cercy, KM, Cerin, E, Chandan, JS, Chang, K-L, Charlson, FJ, Chattu, VK, Chaturvedi, S, Cherbuin, N, Chimed-Ochir, O, Cho, DY, Choi, J-YJ, Christensen, H, Chu, D-T, Chung, MT, Chung, S-C, Cicuttini, FM, Ciobanu, LG, Cirillo, M, Classen, TKD, Cohen, AJ, Compton, K, Cooper, OR, Costa, VM, Cousin, E, Cowden, RG, Cross, DH, Cruz, JA, Dahlawi, SMA, Damasceno, AAM, Damiani, G, Dandona, L, Dandona, R, Dangel, WJ, Danielsson, A-K, Dargan, PI, Darwesh, AM, Daryani, A, Das, JK, Das Gupta, R, das Neves, J, Dávila-Cervantes, CA, Davitoiu, DV, De Leo, D, Degenhardt, L, DeLang, M, Dellavalle, RP, Demeke, FM, Demoz, GT, Demsie, DG, Denova-Gutiérrez, E, Dervenis, N, Dhungana, GP, Dianatinasab, M, Dias da Silva, D, Diaz, D, Dibaji Forooshani, ZS, Djalalinia, S, Do, HT, Dokova, K, Dorostkar, F, Doshmangir, L, Driscoll, TR, Duncan, BB, Duraes, AR, Eagan, AW, Edvardsson, D, El Nahas, N, El Sayed, I, El Tantawi, M, Elbarazi, I, Elgendy, IY, El-Jaafary, SI, Elyazar, IR, Emmons-Bell, S, Erskine, HE, Eskandarieh, S, Esmaeilnejad, S, Esteghamati, A, Estep, K, Etemadi, A, Etisso, AE, Fanzo, J, Farahmand, M, Fareed, M, Faridnia, R, Farioli, A. Faro, A. Faruque, M. Farzadfar, F. Fattahi, N, Fazlzadeh, M, Feigin, VL, Feldman, R, Fereshtehnejad, S-M, Fernandes, E, Ferrara, G, Ferrari, AJ, Ferreira, ML, Filip, I, Fischer, F, Fisher, JL, Flor, LS, Foigt, NA, Folayan, MO, Fomenkov, AA, Force, LM, Foroutan, M, Franklin, RC, Freitas, M, Fu, W, Fukumoto, T, Furtado, JM, Gad, MM, Gakidou, E, Gallus, S, Garcia-Basteiro, AL, Gardner, WM, Geberemariyam, BS, Gebreslassie, AAAA, Geremew, A, Gershberg Hayoon, A, Gething, PW, Ghadimi, M, Ghadiri, K, Ghaffarifar, F, Ghafourifard, M, Ghamari, F, Ghashghaee, A, Ghiasvand, H, Ghith, N, Gholamian, A, Ghosh, R, Gill, PS, Ginindza, TGG, Giussani, G, Gnedovskaya, EV, Goharinezhad, S, Gopalani, SV, Gorini, G, Goudarzi, H, Goulart, AC, Greaves, F, Grivna, M, Grosso, G, Gubari, MIM, Gugnani, HC, Guimarães, RA, Guled, RA, Guo, G, Guo, Y, Gupta, R, Gupta, T, Haddock, B, Hafezi-Nejad, N, Hafiz, A, Haj-Mirzaian, Arvin, Haj-Mirzaian, Arya, Hall, BJ, Halvaei, I, Hamadeh, RR, Hamidi, S, Hammer, MS, Hankey, GJ, Haririan, H, Haro, JM, Hasaballah, AI, Hasan, MM, Hasanpoor, E, Hashi, A, Hassanipour, S, Hassankhani, H, Havmoeller, RJ, Hay, SI, Hayat, K, Heidari, G, Heidari-Soureshjani, R, Henrikson, HJ, Herbert, ME, Herteliu, C, Heydarpour, F, Hird, TR, Hoek, HW, Holla, R, Hoogar, P, Hosgood, HD, Hossain, N, Hosseini, M, Hosseinzadeh, M, Hostiuc, M, Hostiuc, S, Househ, M, Hsairi, M, Hsieh, VC, Hu, G, Hu, K, Huda, TM, Humayun, A, Huynh, CK, Hwang, B-F, Iannucci, VC, Ibitoye, SE, Ikeda, N, Ikuta, KS, Ilesanmi, OS, Ilic, IM, Ilic, MD, Inbaraj, LR, Ippolito, H, Igbal, U, Irvani, SSN, Irvine, CMS, Islam, MM, Islam, SMS, Iso, H, Ivers, RQ, Iwu, CCD, Iwu, CJ, Iyamu, IO, Jaafari, J, Jacobsen, KH, Jafari, H, Jafarinia, M, Jahani, MA, Jakovljevic, M, Jalilian, F, James, SL, Janjani, H, Javaheri, T, Javidnia, J, Jeemon, P, Jenabi, E, Jha, RP, Jha, V, Ji, JS, Johansson, L, John, O, John-Akinola, YO, Johnson, CO, Jonas, JB, Joukar, F, Jozwiak, JJ, Jürisson, M, Kabir, A, Kabir, Z, Kalani, H, Kalani, R, Kalankesh, LR, Kalhor, R, Kanchan, T, Kapoor, N, Karami Matin, B, Karch, A, Karim, MA, Kassa, GM, Katikireddi, SV, Kayode, GA, Kazemi Karyani, A, Keiyoro, PN, Keller, C, Kemmer, L, Kendrick, PJ, Khalid, N, Khammarnia, M, Khan, EA, Khan, M, Khatab, K, Khater, MM, Khatib, MN, Khayamzadeh, M, Khazaei, S, Kieling, C, Kim, YJ, Kimokoti, RW, Kisa, A, Kisa, S, Kivimäki, M, Knibbs, LD, Knudsen, AKS, Kocarnik, JM, Kochhar, S, Kopec, JA, Korshunov, VA, Koul, PA, Koyanagi, A, Kraemer, MUG, Krishan, K, Krohn, KJ, Kromhout, H, Kuate Defo, B, Kumar, GA, Kumar, V, Kurmi, OP, Kusuma, D, La Vecchia, C, Lacey, B, Lal, DK, Lalloo, R, Lallukka, T, Lami, FH, Landires, I, Lang, JJ, Langan, SM, Larsson, AO, Lasrado, S, Lauriola, P, Lazarus, JV, Lee, PH, Lee, SWH, LeGrand, KE, Leigh, J, Leonardi, M, Lescinsky, H, Leung, J, Levi, M, Li, S, Lim, L-L, Linn, S, Liu, Shiwei, Liu, Simin, Liu, Y, Lo, J, Lopez, AD, Lopez, JCF, Lopukhov, PD, Lorkowski, S, Lotufo, PA, Lu, A, Lugo, A, Maddison, ER, Mahasha, PW, Mahdavi, MM, Mahmoudi, M, Majeed, A, Maleki, A, Maleki, S, Malekzadeh, R, Malta, DC, Mamun, AA, Manda, AL, Manguerra, H, Mansour-Ghanaei, F, Mansouri, B, Mansournia, MA, Mantilla Herrera, AM, Maravilla, JC, Marks, A, Martin, RV, Martini, S, Martins-Melo, FR, Masaka, A, Masoumi, SZ, Mathur, MR, Matsushita, K, Maulik, PK, McAlinden, C, McGrath, JJ, McKee, M, Mehndiratta, MM, Mehri, F, Mehta, KM, Memish, ZA, Mendoza, W, Menezes, RG, Mengesha, EW, Mereke, A, Mereta, ST, Meretoja, A, Meretoja, TJ, Mestrovic, T, Miazgowski, B, Miazgowski, T, Michalek, IM, Miller, TR, Mills, EJ, Mini, G, Miri, M, Mirica, A, Mirrakhimov, EM, Mirzaei, H, Mirzaei, M, Mirzaei, R, Mirzaei-Alavijeh, M, Misganaw, AT, Mithra, P, Moazen, B, Mohammad, DK, Mohammad, Y, Mohammad Gholi Mezerji, N, Mohammadian-Hafshejani, A, Mohammadifard, N, Mohammadpourhodki, R, Mohammed, AS, Mohammed, H, Mohammed, JA, Mohammed, S, Mokdad, AH, Molokhia, M,

Monasta, L, Mooney, MD, Moradi, G, Moradi, M, Moradi-Lakeh, M, Moradzadeh, R, Moraga, P, Morawska, L, Morgado-da-Costa, J, Morrison, SD, Mosapour, A, Mosser, JF, Mouodi, S, Mousavi, SM, Mousavi Khaneghah, A, Mueller, UO, Mukhopadhyay, S, Mullany, EC, Musa, KI, Muthupandian, S, Nabhan, AF, Naderi, M, Nagarajan, AJ, Nagel, G, Naghavi, M, Naghshtabrizi, B, Naimzada, MD, Najafi, F, Nangia, V, Nansseu, JR, Naserbakht, M, Nayak, VC, Negoi, I, Ngunjiri, JW, Nguyen, CT, Nguyen, HLT, Nguyen, M, Nigatu, YT, Nikbakhsh, R, Nixon, MR, Nnaji, CA, Nomura, S, Norrving, B, Noubiap, JJ, Nowak, C, Nunez-Samudio, V, Oţoiu, A, Oancea, B, Odell, CM, Ogbo, FA, Oh, I-H, Okunga, EW, Oladnabi, M, Olagunju, AT, Olusanya, BO, Olusanya, JO, Omer, MO, Ong, KL, Onwujekwe, OE, Orpana, HM, Ortiz, A, Osarenotor, O, Osei, FB, Ostroff, SM, Otstavnov, N, Otstavnov, SS, Øverland, S, Owolabi, MO, PA, M, Padubidri, JR, Palladino, R, Panda-Jonas, S, Pandey, A, Parry, CDH, Pasovic, M, Pasupula, DK, Patel, SK, Pathak, M, Patten, SB, Patton, GC, Pazoki Toroudi, H, Peden, AE, Pennini, A, Pepito, VCF, Peprah, EK, Pereira, DM, Pesudovs, K, Pham, HQ, Phillips, MR, Piccinelli, C, Pilz, TM, Piradov, MA, Pirsaheb, M, Plass, D, Polinder, S, Polkinghorne, KR, Pond, CD, Postma, MJ, Pourjafar, H, Pourmalek, F, Poznańska, A, Prada, SI, Prakash, V, Pribadi, DRA, Pupillo, E, Quazi Syed, Z, Rabiee, M, Rabiee, N, Radfar, A, Rafiee, A, Raggi, A, Rahman, MA, Rajabpour-Sanati, A, Rajati, F, Rakovac, I, Ram, P, Ramezanzadeh, K, Ranabhat, CL, Rao, PC, Rao, SJ, Rashedi, V, Rathi, P, Rawaf, DL, Rawaf, S, Rawal, L, Rawassizadeh, R, Rawat, R, Razo, C, Redford, SB, Reiner, RC, Reitsma, MB, Remuzzi, G, Renjith, V. Renzaho, AMN, Resnikoff, S. Rezaei, Negar, Rezaei, Nima, Rezapour, A, Rhinehart, P-A, Riahi, SM, Ribeiro, DC, Ribeiro, D, Rickard, J, Rivera, JA, Roberts, NLS, Rodríguez-Ramírez, S, Roever, L, Ronfani, L, Room, R, Roshandel, G, Roth, GA, Rothenbacher, D, Rubagotti, E, Rwegerera, GM, Sabour, S, Sachdev, PS, Saddik, B, Sadeghi, E, Sadeghi, M, Saeedi, R, Saeedi Moghaddam, S, Safari, Y, Safi, S, Safiri, S, Sagar, R, Sahebkar, A, Sajadi, SM, Salam, N, Salamati, P, Salem, H, Salem, MRR, Salimzadeh, H, Salman, OM, Salomon, JA, Samad, Z, Samadi Kafil, H, Sambala, EZ, Samy, AM, Sanabria, J, Sánchez-Pimienta, TG, Santomauro, DF, Santos, IS, Santos, JV, Santric-Milicevic, MM, Saraswathy, SYI, Sarmiento-Suárez, R, Sarrafzadegan, N, Sartorius, B, Sarveazad, A, Sathian, B, Sathish, T, Sattin, D, Saxena, S, Schaeffer, LE, Schiavolin, S, Schlaich, MP, Schmidt, MI, Schutte, AE, Schwebel, DC, Schwendicke, F, Senbeta, AM, Senthilkumaran, S, Sepanlou, SG, Serdar, B, Serre, ML, Shadid, J, Shafaat, O, Shahabi, S, Shaheen, AA, Shaikh, MA, Shalash, AS, Shams-Beyranvand, M, Shamsizadeh, M, Sharafi, K, Sheikh, A,

Sheikhtaheri, A, Shibuya, K, Shield, KD, Shigematsu, M, Shin, JI, Shin, M-J, Shiri, R, Shirkoohi, R, Shuval, K, Siabani, S, Sierpinski, R, Sigfusdottir, ID, Sigurvinsdottir, R, Silva, JP, Simpson, KE, Singh, JA, Singh, P, Skiadaresi, E, Skou, STS, Skryabin, VY, Smith, EUR, Soheili, A, Soltani, S, Soofi, M, Sorensen, RJD, Soriano, JB, Sorrie, MB, Soshnikov, S, Soyiri, IN, Spencer, CN, Spotin, A, Sreeramareddy, CT, Srinivasan, V, Stanaway, JD, Stein, C, Stein, DJ, Steiner, C, Stockfelt, L, Stokes, MA, Straif, K, Stubbs, JL, Sufiyan, MB, Suleria, HAR, Suliankatchi Abdulkader, R, Sulo, G, Sultan, I, Szumowski, Ł, Tabarés-Seisdedos, R, Tabb, KM, Tabuchi, T, Taherkhani, A, Tajdini, M, Takahashi, K, Takala, JS, Tamiru, AT, Taveira, N, Tehrani-Banihashemi, A, Temsah, M-H, Tesema, GA, Tessema, ZT, Thurston, GD, Titova, MV, Tohidinik, HR, Tonelli, M, Topor-Madry, R, Topouzis, F, Torre, AE, Touvier, M, Tovani-Palone, MRR, Tran, BX, Travillian, R, Tsatsakis, A, Tudor Car, L, Tyrovolas, S, Uddin, R, Umeokonkwo, CD, Unnikrishnan, B, Upadhyay, E, Vacante, M, Valdez, PR, van Donkelaar, A, Vasankari, TJ, Vasseghian, Y, Veisani, Y, Venketasubramanian, N, Violante, FS, Vlassov, V, Vollset, SE, Vos, T, Vukovic, R, Waheed, Y, Wallin, MT, Wang, Y, Wang, Y-P, Watson, A, Wei, J, Wei, MYW, Weintraub, RG, Weiss, J, Werdecker, A, West, JJ, Westerman, R, Whisnant, JL, Whiteford, HA, Wiens, KE, Wolfe, CDA, Wozniak, SS, Wu, A-M, Wu, J, Wulf Hanson, S, Xu, G, Xu, R, Yadgir, S, Yahyazadeh Jabbari, SH, Yamagishi, K, Yaminfirooz, M, Yano, Y, Yaya, S, Yazdi-Feyzabadi, V, Yeheyis, TY, Yilgwan, CS, Yilma, MT, Yip, P, Yonemoto, N, Younis, MZ, Younker, TP, Yousefi, B, Yousefi, Z, Yousefinezhadi, T, Yousuf, AY, Yu, C, Yusefzadeh, H, Zahirian Moghadam, T, Zamani, M, Zamanian, M, Zandian, H, Zastrozhin, MS, Zhang, Y, Zhang, Z-J, Zhao, JT, Zhao, X-JG, Zhao, Y, Zhou, M, Ziapour, A, Zimsen, SRM, Brauer, M, Afshin, A, Lim, SS. 2020. Global burden of 87 risk factors in 204 countries and territories, 1990-2019: A systematic analysis for the global burden of disease study 2019. The Lancet **396**: 1223–1249. DOI: http://dx.doi.org/10.1016/ S0140-6736(20)30752-2.

Murray, LT, Jacob, DJ, Logan, JA, Hudman, RC, Koshak, WJ. 2012. Optimized regional and interannual variability of lightning in a global chemical transport model constrained by LIS/OTD satellite data. *Journal of Geophysical Research Atmospheres* 117. DOI: http://dx.doi.org/10.1029/2012JD017934.

Nault, BA, Jo, DS, McDonald, BC, Campuzano-Jost, P, Day, DA, Hu, W, Schroder, JC, Allan, J, Blake, DR, Canagaratna, MR, Coe, H, Coggon, MM, DeCarlo, PF, Diskin, GS, Dunmore, R, Flocke, F, Fried, A, Gilman, JB, Gkatzelis, G, Hamilton, JF, Hanisco, TF, Hayes, PL, Henze, DK, Hodzic, A, Hopkins, J, Hu, M, Huey, LG, Jobson, BT, Kuster, WC, Lewis, A, Li, M, Liao, J, Nawaz, MO, Pollack, IB, Peischl, J, Rappenglück, B, Reeves, CE, Richter, D,

- Roberts, JM, Ryerson, TB, Shao, M, Sommers, JM, Walega, J, Warneke, C, Weibring, P, Wolfe, GM, Young, DE, Yuan, B, Zhang, Q, de Gouw, JA, Jimenez, JL. 2020. Anthropogenic secondary organic aerosols contribute substantially to air pollution mortality. *Atmospheric Chemistry and Physics* 1–53. DOI: http://dx.doi.org/10.5194/acp-2020-914.
- Nawaz, MO, Henze, DK. 2020. Premature deaths in Brazil associated with long-term exposure to PM2.5 from amazon fires between 2016 and 2019. *Geo-Health* **4**: e2020GH000268. DOI: http://dx.doi.org/10.1029/2020GH000268.
- Ni, R, Lin, J, Yan, Y, Lin, W. 2018. Foreign and domestic contributions to springtime ozone over China. *Atmospheric Chemistry and Physics* **18**: 11447–11469. DOI: http://dx.doi.org/10.5194/acp-18-11447-2018.
- Nopmongcol, U, Liu, Z, Stoeckenius, T, Yarwood, G. 2017. Modeling intercontinental transport of ozone in North America with CAMx for the air quality model evaluation international initiative (AQMEII) Phase 3. *Atmospheric Chemistry and Physics* 17: 9931–9943. DOI: http://dx.doi.org/10.5194/acp-17-9931-2017.
- Pappin, AJ, Hakami, A. 2013. Source attribution of health benefits from air pollution abatement in Canada and the United States: An adjoint sensitivity analysis. *Environmental Health Perspectives* 121: 572–579. DOI: http://dx.doi.org/10.1289/ehp. 1205561.
- Punger, EM, West, JJ. 2013. The effect of grid resolution on estimates of the burden of ozone and fine particulate matter on premature mortality in the United States. Air Quality, Atmosphere & Health 6. DOI: http://dx.doi.org/10.1007/s11869-013-0197-8.
- **Ridder de, K, Viaene, P, Van de Vel, K, Brasseur, O, Cheymol, A, Fierens, F.** 2014. The impact of model resolution on simulated ambient air quality and associated human exposure. *Atmósfera* **27**: 403–410. DOI: http://dx.doi.org/10.1016/S0187-6236(14)70038-4.
- Romer Present, PS, Zare, A, Cohen, RC. 2020. The changing role of organic nitrates in the removal and transport of NO_x. *Atmospheric Chemistry and Physics* **20**: 267–279. DOI: http://dx.doi.org/10.5194/acp-20-267-2020.
- Russell, MC, Belle, JH, Liu, Y. 2017. The impact of three recent coal-fired power plant closings on Pittsburgh air quality: A natural experiment. *Journal of the Air & Waste Management Association* 67: 3–16. DOI: http://dx.doi.org/10.1080/10962247.2016. 1170738.
- **Seinfeld, JH, Pandis, SN**. 2016. *Atmospheric chemistry and physics: From air pollution to climate change.* New York, NY: John Wiley & Sons, Inc.
- Shaddick, G, Thomas, ML, Green, A, Brauer, M, van Donkelaar, A, Burnett, R, Chang, HH, Cohen, A, Dingenen, RV, Dora, C, Gumy, S, Gumy, S, Liu, Y, Martin, R, Waller, LA, West, J, Zidek, JV, Prüss-

- **Ustün, A**. 2018. Data integration model for air quality: A hierarchical approach to the global estimation of exposures to ambient air pollution. *Journal of the Royal Statistical Society: Series C (Applied Statistics)* **67**: 231–253. DOI: http://dx.doi.org/10.1111/rssc. 12227
- Stauffer, RM, Thompson, AM, Martins, DK, Clark, RD, Goldberg, DL, Loughner, CP, Delgado, R, Dickerson, RR, Stehr, JW, Tzortziou, MA. 2015. Bay breeze influence on surface ozone at Edgewood, MD during July 2011. *Journal of Atmospheric Chemistry* **72**: 335–353. DOI: http://dx.doi.org/10.1007/s10874-012-9241-6.
- Sullivan, JT, Berkoff, T, Gronoff, G, Knepp, T, Pippin, M, Allen, D, Twigg, L, Swap, R, Tzortziou, M, Thompson, AM, Stauffer, RM, Wolfe, GM, Flynn, J, Pusede, SE, Judd, LM, Moore, W, Baker, BD, Al-Saadi, J, McGee, TJ. 2019. The ozone water—land environmental transition study: An innovative strategy for understanding Chesapeake Bay pollution events. *Bulletin of the American Meteorological Society* 100: 291–306. DOI: http://dx.doi.org/10.1175/BAMS-D-18-0025.1.
- Thurston, GD., Ito, K, Lall, R. 2011. A source apportionment of U.S. fine particulate matter air pollution. *Atmospheric Environment Oxford, England 1994* **45**: 3924–3936. DOI: http://dx.doi.org/10.1016/j. atmosenv.2011.04.070.Travis, KR, Jacob, DJ. 2019. Systematic bias in evaluating chemical transport models with maximum daily 8 h average (MDA8) surface ozone for air quality applications: a case study with GEOS-Chem v9.02. *Geoscientific Model Development* **12**: 3641–3648. DOI: http://dx.doi.org/10.5194/gmd-12-3641-2019.
- Travis, KR, Jacob, DJ, Fisher, JA, Kim, PS, Marais, EA, Zhu, L, Yu, K, Miller, CC, Yantosca, RM, Sulprizio, MP, Thompson, AM, Wennberg, PO, Crounse, JD, St Clair, JM, Cohen, RC, Laughner, JL, Dibb, JE, Hall, SR, Ullmann, K, Wolfe, GM, Pollack, IB, Peischl, J, Neuman, JA, Zhou, X. 2016. Why do models overestimate surface ozone in the Southeast United States? *Atmospheric Chemistry and Physics* 16: 13561–13577. DOI: http://dx.doi.org/10.5194/acp-16-13561-2016.
- Turner, MC, Jerrett, M, Pope, III CA, Krewski, D, Gapstur, SM, Diver, WR, Beckerman, BS, Marshall, JD, Su, J, Crouse, DL, Burnett, RT. 2016. Long-term ozone exposure and mortality in a large prospective study. *American Journal of Respiratory and Critical Care Medicine* 193: 1134–1142. DOI: http://dx.doi.org/10.1164/rccm.201508-1633OC.
- Turnock, ST, Allen, RJ, Andrews, M, Bauer, SE, Deushi, M, Emmons, L, Good, P, Horowitz, L, John, JG, Michou, M, Nabat, P, Naik, V, Neubauer, D, O'Connor, FM, Olivié, D, Oshima, N, Schulz, M, Sellar, A, Shim, S, Takemura, T, Tilmes, S, Tsigaridis, K, Wu, T, Zhang, J. 2020. Historical and future changes in air pollutants from CMIP6 models. *Atmospheric Chemistry and Physics* 20: 14547–14579.

DOI: http://dx.doi.org/10.5194/acp-20-14547-2020.

- United Nations, Department of Economic and Social Affairs, Population Division. 2019. World urbanization prospects: The 2018 revision. Available at https://population.un.org/wup/Publications/Files/WUP2018-Report.pdf.
- **U.S. Environmental Protection Agency**. 2014. NAAQS Table [WWW document]. U.S. Environmental Protection Agency. Available at https://www.epa.gov/criteria-air-pollutants/naaqs-table. Accessed 11 September 2020.
- U.S. Environmental Protection Agency. 2015. Table of historical ozone national ambient air quality standards (NAAQS) [WWW document]. U.S. Environmental Protection Agency. Available at https://www.epa. gov/ground-level-ozone-pollution/table-historicalozone-national-ambient-air-quality-standards-naaqs. Accessed 1 November 2021.
- Van der Werf, GR, Randerson, JT, Giglio, L, Collatz, GJ, Mu, M, Kasibhatla, PS, Morton, DC, DeFries, RS, Jin, YV, van Leeuwen, TT. 2010. Global fire emissions and the contribution of deforestation, savanna, forest, agricultural, and peat fires (1997–2009). Atmospheric Chemistry and Physics 10: 11707–11735. DOI: http://dx.doi.org/10.5194/acp-10-11707-2010.
- Van Donkelaar, A, Martin, RV, Brauer, M, Hsu, NC, Kahn, RA, Levy RC, Lyapustin, A, Sayer, AM, Winker, DM. 2016. Global estimates of fine

- particulate matter using a combined geophysical-statistical method with information from satellites, models, and monitors. *Environmental Science & Technology* **50**: 3762–3772. DOI: http://dx.doi.org/10.1021/acs.est.5b05833.
- World Health Organization. 2021. Ambient Air Pollution [WWW document]. World Health Organization. Available at https://www.who.int/data/gho/data/themes/topics/topic-details/GHO/ambient-air-pollution. Accessed 16 August 2021.
- **Zender, CS, Bian, H, Newman, D**. 2003. Mineral dust entrainment and deposition (DEAD) model: description and 1990s dust climatology. *Journal of Geophysical Research Atmospheres* **108**. DOI: http://dx.doi.org/10.1029/2002JD002775.
- Zhang, L, Liu, L, Zhao, Y, Gong, S, Zhang, X, Henze, DK, Capps, SL, Fu, TM, Zhang, Q, Wang, Y. 2015. Source attribution of particulate matter pollution over North China with the adjoint method. *Environmental Research Letters* 10: 084011. DOI: http://dx.doi.org/10.1088/1748-9326/10/8/084011.
- Zhang, Y, West, JJ, Mathur, R, Xing, J, Hogrefe, C, Roselle, SJ, Bash, JO, Pleim, JE, Gan, C-M, Wong, DC. 2018. Long-term trends in the ambient PM_{2.5}- and O₃-related mortality burdens in the United States under emission reductions from 1990 to 2010. *Atmospheric Chemistry and Physics* **18**: 15003–15016. DOI: http://dx.doi.org/10.5194/acp-18-15003-2018.

How to cite this article: Nawaz, MO, Henze, DK, Harkins, C, Cao, H, Nault, B, Jo, D, Jimenez, J, Anenberg, SC, Goldberg, DL, Qu, Z. 2021. Impacts of sectoral, regional, species, and day-specific emissions on air pollution and public health in Washington, DC. *Elementa: Science of the Anthropocene* 9(1). DOI: https://doi.org/10.1525/elementa.2021.00043

Domain Editor-in-Chief: Detlev Helmig, Boulder AIR LLC, Boulder, CO, USA

Associate Editor: Gabriele Pfister, National Center for Atmospheric Research, Boulder, CO, USA

Knowledge Domain: Atmospheric Science

Published: December 13, 2021 Accepted: November 12, 2021 Submitted: June 7, 2021

Copyright: © 2021 The Author(s). This is an open-access article distributed under the terms of the Creative Commons Attribution 4.0 International License (CC-BY 4.0), which permits unrestricted use, distribution, and reproduction in any medium, provided the original author and source are credited. See http://creativecommons.org/licenses/by/4.0/.

